Phenotyping heart failure using model-based analysis and physiology-informed machine learning

Edith Jones[1], E. Benjamin Randall[1], Scott L. Hummel[2, 3], David Cameron[2], Daniel A. Beard[1] and Brian E. Carlson[1]

[1]Department of Molecular and Integrative Physiology, University of Michigan, Ann Arbor, MI 48109
[2]Department of Cardiovascular Medicine, University of Michigan, Ann Arbor, MI 48109
[3]Ann Arbor Veterans Affairs Health System, Ann Arbor, MI 48105

Key Points

1. Analysis of data from RHC and TTE of HF patients using a closed-loop model of the cardiovascular system identifies key parameters representing hemodynamic cardiovascular function in HFrEF and HFpEF patients.

2. Analyzing optimized parameters representing cardiovascular function using machine learning shows mechanistic differences between HFpEF groups that are not seen analyzing clinical data alone.

3. HFpEF groups presented here can be subdivided into 3 subgroups: HFpEF1 described as "HFrEF-like HFpEF", HFpEF2 as "pure HFpEF", and a third group of HFpEF patients that do not consistently cluster.

4. Focusing purely on cardiac function consistently captures the underlying dysfunction in HFrEF, whereas HFpEF is better characterized by dysfunction in the entire cardiovascular system.

5. Our methodology reveals that elevated left ventricular systolic and diastolic volumes are potential biomarkers for identifying HFpEF-like HFrEF patients.

Abstract

To phenotype mechanistic differences between heart failure with reduced (HFrEF) and preserved (HFpEF) ejection fraction, a closed-loop model of the cardiovascular system coupled with patient-specific transthoracic echocardiography (TTE) and right heart catheterization (RHC) data was used to identify key parameters representing hemodynamics. Thirty-one patient records (10 HFrEF, 21 HFpEF) were obtained from the Cardiovascular Health Improvement Project database at the University of Michigan. Model simulations were tuned to match RHC and TTE pressure, volume, and cardiac output measurements in each patient. The underlying physiological model parameters were plotted against model-based norms and compared between HFrEF and HFpEF. Our results confirm the main mechanistic parameter driving HFrEF is reduced left ventricular (LV) contractility, whereas HFpEF exhibits a heterogeneous phenotype. Conducting principal component analysis, k-means

clustering, and hierarchical clustering on the optimized parameters reveal (i) a group of HFrEF-like HFpEF patients (HFpEF1), (ii) a "pure" HFpEF group (HFpEF2), and (iii) a group of HFpEF patients that do not consistently cluster (NCC). These subgroups cannot be distinguished from the clinical data alone. Increased LV active contractility ($\Box$-value<0.001) and LV passive stiffness ($\Box$-value<0.001) at rest are observed when comparing HFpEF2 to HFpEF1. Analyzing the clinical data of each subgroup reveals that elevated systolic and diastolic LV volumes seen in both HFrEF and HFpEF1 may be used as a biomarker to identify HFrEF-like HFpEF patients. These results suggest that modeling of the cardiovascular system and optimizing to standard clinical data can designate subgroups of HFpEF as separate phenotypes, possibly elucidating patient-specific treatment strategies.

Keywords: preserved ejection fraction, reduced ejection fraction, clinical data, cardiovascular systems modeling, k-means clustering, hierarchical clustering

Running Title: Phenotyping heart failure with modeling analysis and machine learning

Corresponding Author:
Brian E. Carlson, PhD
Department of Molecular and Integrative Physiology
University of Michigan
2800 Plymouth Road
NCRC B10/A126
Ann Arbor, Michigan 48109
email: bcarl@umich.edu
phone: (734) 763-8057

About the Authors

Edith Jones earned her Bachelor of Science in Biology with a minor in Biochemistry at the University of Texas-Rio Grande Valley. She is now working on her PhD at the University of Michigan where her experience in the labs of Daniel Beard and Brian Carlson has allowed her to study both cardiovascular metabolism as well as hemodynamics using biochemical and computational modeling approaches. She hopes to use her background in physiology to understand metabolic pathology from a systems biology perspective.

Dr. **E. Benjamin Randall** earned his Ph.D. in Applied Mathematics from North Carolina State University with a minor in Physiology in 2019 under the direction of Mette S. Olufsen, Ph.D. He is currently a T32 Postdoctoral Fellow at the University of Michigan working with Daniel A. Beard, Ph.D. and Brian E. Carlson, Ph.D. His area of expertise lies in the development and analysis of patient-specific mathematical models investigating individual cardiovascular and cardiac function, e.g., the methodology introduced in this study.

Introduction

Heart Failure with preserved ejection fraction (HFpEF) is diagnosed in patients with the hallmarks of heart failure (HF) and a left ventricular (LV) ejection fraction (EF) equal to or above 50%. HFpEF now represents more than half of HF cases, and its incidence is increasing with an aging population and a high prevalence of associated risk factors (e.g., obesity, systemic hypertension, coronary artery disease, and diabetes) (Yancy *et al.*, 2006; Owan *et al.*, 2006; Hummel *et al.*, 2009; Little & Zile, 2012). Patients with HFpEF suffer poor quality of life and long-term outcomes. Despite this substantial individual and public health burden, HFpEF lacks a framework for evidence-based pharmacotherapy (Yancy *et al.*, 2013). Long-term management of HFpEF focuses on (i) the treatment of any existing comorbidities, (ii) therapeutics that decrease the LV diastolic pressures, and (iii) general symptom reduction. Several clinical trials in large cohorts of HFpEF patients have failed to demonstrate consistent benefits. The drugs used include sildenafil (Guazzi *et al.*, 2011; Borlaug *et al.*, 2015; Hoendermis *et al.*, 2015; Liu *et al.*, 2017), sacubitril/valsartan (Solomon *et al.*, 2019), losartan (Wachtell *et al.*, 2010), candesartan (Yusuf *et al.*, 2003), spironolactone (Edelmann *et al.*, 2013; Cohen *et al.*, 2020a), and isosorbide mononitrate (Redfield *et al.*, 2015).

HFpEF was previously termed "diastolic" HF with symptoms attributed to increased ventricular stiffness, impaired relaxation, impaired ventricular filling during diastole, and higher average pressures during the cardiac cycle. However, patients with HFpEF have dysfunction in multiple cardiovascular domains, some of which may become evident only during exercise (Dunlay *et al.*, 2017). It has been suggested that selecting the correct HFpEF cohort is an important factor in treatment success (Borlaug *et al.*, 2015), but the wide range of HFpEF phenotypes at the mechanistic cardiovascular systems level makes selecting these cohorts from upper-level clinical data difficult. Since HFpEF is a catch-all category for HF patients based mainly on EF estimates, the inability to have a standard treatment for these patients may be an indicator of the physiological heterogeneity underlying HFpEF. Therefore, identifying subgroups of HFpEF patients with similar cardiovascular etiologies is a crucial task required to target appropriate therapies for these patients.

Patients presenting with HF and an EF below 50% are diagnosed with heart failure with reduced ejection fraction (HFrEF). The classical understanding of HFrEF, also known as "systolic" HF, is that loss of ventricular contractility causes reduced ability to pump blood to the systemic circulation during systole (Pinilla-Vera *et al.*, 2019). Unlike HFpEF, numerous medication and device-based therapies improve outcomes in HFrEF (Yancy *et al.*, 2017; Pinilla-Vera *et al.*, 2019) .

To diagnose and monitor patients with HF, two clinical procedures are commonly used: transthoracic echocardiography (TTE) and right heart catheterization (RHC). TTE is noninvasive and widely available, and these images may be used to quantify LV volumes in systole and diastole to estimate a patient's EF. From TTE measurements, we may obtain additional information, such as cardiac output (CO) based on the heart rate (HR), the left ventricular out track flow velocity time integral (LVOT VTI) and the cross-sectional aortic valve area for each patient. RHC is used to measure right ventricular (RV) and pulmonary artery (PA) pressures during systole and diastole along with CO, HR, and pulmonary capillary wedge pressure (PCW). While TTE and RHC provide detailed ventricular volume and pressure data for individual patients, the challenge of integrating these measurements into a single representation of a patient's cardiovascular state is only made qualitatively in the clinic. One way to quantitatively reconcile what these clinical datasets describe about the hemodynamics of the

right and left sides of the heart and the systemic and pulmonary circulation is with a closed-loop model of the cardiovascular system. To combine these two sets of data, we must take into consideration that (i) the two datasets are typically not obtained simultaneously, (ii) they may include a combination of data points taken at specific instances, and (iii) time course data are often not available.

In this retrospective study, we have developed a methodology to represent the cardiovascular state of both HFpEF and HFrEF patients to illustrate the underlying mechanistic differences between diagnoses and specifically within the diagnosis of HFpEF. Recent studies have determined subgroups of the HFpEF diagnosis using RNA sequencing (Hahn *et al.*, 2021), quantitative echocardiography (Shah, 2019), and plasma protein profiling (Cohen *et al.*, 2020*b*) combined with unsupervised machine learning techniques.

Here, we aim to discern subgroups within the HFpEF cohort using a mathematical modeling and unsupervised machine learning approach. To this end, a clustering analysis is performed on estimated model parameters identifying HFpEF subgroups that provide hemodynamic insight into functional differences between HFpEF subgroups. Others have attempted to classify HF patients using clinical data to inform cardiovascular modeling (Wang *et al.*, 2018). To our knowledge, ours is the first study that uses model-based analysis of clinical data and physiology-informed machine learning to determine subclassifications of HFpEF. This synergistic approach is in line with similar studies that combine mathematical and statistical techniques to predict physiological function at the patient-specific level (e.g., the "digital twin" (Corral-Acero *et al.*, 2020)). A workflow of the approach used in this study is shown in **Figure 1**.

<p align="center">**FIGURE 1 HERE - METHODOLOGY**</p>

Methods

Clinical Data

The Cardiovascular Health Improvement Project (CHIP) repository, supported by the Frankel Cardiovascular Center at the University of Michigan, was queried to extract clinical data from patients diagnosed with HFpEF or HFrEF. This retrospective data capture was approved by the Institutional Review Board at the University of Michigan, and informed consent was obtained for all subjects in the database. This research-ready biorepository of DNA, plasma, serum, and tissue samples includes de-identified electronic health records (EHRs) from consenting patients with HF, aortic disease, arrhythmia, and dyslipidemia. Through the CHIP office, a search was made to collect clinical data from HFpEF and HFrEF patients with both TTE and RHC measurements in their EHR. The criteria for determining whether a patient has HFpEF or HFrEF is a history of HF symptoms and an EF above 50% or below 50%, respectively. Patients with both procedures within 90 days of each other were extracted from all HFpEF and HFrEF records in a time range from February 2016 through February 2019. With this query, 62 patient records (26 HFrEF and 36 HFpEF) were collected. Patient records missing the minimal number of measurements (see below) from RHC and TTE procedures eliminated 10 HFrEF and 13 HFpEF records, leaving 34 patient records (11 HFrEF and 23 HFpEF). Finally, one HFrEF and two HFpEF records that appeared to be outliers during the initial phase of our analysis were followed up in the patient record and found to have procedures or treatments that changed their

original cardiovascular diagnosis (e.g., chemotherapy changing a patient from HFpEF to HFrEF). These three patients were omitted from our final analysis, leaving 31 patient records (10 HFrEF and 21 HFpEF).

RHC data: During this invasive procedure, a Swan-Ganz catheter is inserted through the jugular vein and measures the pressure at the tip of the catheter as it is advanced into the pulmonary artery. Besides pressure information, CO is estimated by using the thermodilution or Fick methods. The thermodilution technique estimates CO by measuring dispersion of a cold saline bolus injected at the proximal end and then sensed at the distal end of the catheter. The Fick method measures venous and arterial O_2 saturation and often assumes a given whole body oxygen consumption ($\dot{V}O_2$) based on weight, height, and sex. The accuracy of the Fick method hinges on correctly estimating $\dot{V}O_2$, and it has been determined that it can vary by as much as 25% when compared to a direct measurement of $\dot{V}O_2$ (Narang *et al.*, 2014). Since all RHC records in this study used estimated $\dot{V}O_2$, we have chosen to use the thermodilution method as a consistent measure of RHC CO.

The selected RHC datasets came from reports that contained at least the following 13 clinically measured values: systolic and diastolic RV pressures, systolic and diastolic PA pressures, average PCW pressure, systolic and diastolic SA pressure, HR during the RHC, CO (thermodilution and Fick), body weight, height, and sex (**Table 1**). To ensure that the RHC measurements used are consistent, HR and systolic and diastolic systemic pressures were gathered from the RHC report only during catheter insertion. If multiple measurements were taken during this period, an average was computed of the values recorded.

TTE data: The selected TTE data include at a minimum: measurements of LV volume in systole and diastole and HR during TTE. The LV volumes are measured as either (i) a single diameter across the LV just below the mitral valve leaflet tips or (ii) tracings of the LV from apical two- and four-chamber views (Lang RM *et al.*, 2016). The single diameter derived volumes assume the LV can be approximated as a truncated prolate spheroid with a nonlinear relationship between the diameter and length of the ventricle (Teichholz *et al.*, 1976). Volumes derived from the two- and four-chamber views are calculated by the Method of Discs (MOD), also known as Simpson's method (Lang RM *et al.* 2016). Since MOD is preferred for the estimation of LV volumes over the single diameter estimation, all patient raw TTE images were reviewed by a cardiologist to:

(i)   Obtain a MOD estimate of LV volumes when the quality of the image allowed,
(ii)   Determine the HR, and
(iii)   Extract an LVOT VTI estimate of CO, when possible.

FIGURE 2 HERE - DECISION TREES

Data discrepancy/inconsistency

Ejection fraction: All patients had a reported EF determined visually by a cardiologist. To quantitively determine the EF, Cameron revisited the TTE images to reassess LV volumes by MOD (EF_{MOD}). There are some patients where the two- and four-chamber images were not of high enough resolution to yield a MOD estimate. In these cases, the LV volumes and CO are calculated from a single diameter measured across the top of the LV using the Teichholz equation (EF_T). (Teichholz *et al.*, 1976). If EF_{MOD} was able to be calculated, we assign this value as EF_1, and if not, $EF_1 = EF_T$. This method revealed discrepancies between the reported EF and EF_1. To address this discrepancy, we had a third evaluation performed by Hummel to determine whether EF_1 should be used. If the distance between the reported EF and EF_1 is less than 0.1, we use EF_1. Otherwise, we apply the rule

$$EF_2 = \frac{SV_{LVOT}}{V_{LV,diast}}, \tag{1}$$

where SV_{LVOT} is the stroke volume (SV) determined by LVOT VTI, and $V_{LV,diast}$ is the diastolic LV volume determined by MOD or Teichholz. If the distance between the reported EF and EF_2 is less than 0.1, we use EF_2. Otherwise, we apply the rule

$$EF_3 = \frac{SV_{LVOT}}{V_{LV,syst} + SV_{LVOT}}, \tag{2}$$

where $V_{LV,syst}$ is the systolic LV volume determined by MOD or Teichholz. The decision tree for the reassessment of EF is shown in **Figure 2A**. Additional details on the EF calculation for each patient is summarized in Section **S2** and **Table S2** of the Supplemental Material.

Cardiac output: Both TTE and RHC data can contain multiple estimates of CO. The TTE itself resulted in a possibility of three separate CO estimates:

(i)   HR times the SV using MOD (CO_{MOD}),

(ii)   HR times the SV using the Teichholz equation (CO_T), and

(iii)   HR times LVOT VTI times the cross-sectional area of the outflow tract (CO_{LVOT}) (Lang RM *et al.*, 2016).

We have developed a systematic method to rank the quality of these measurements and determine a CO estimate to be used for parameter optimization, as shown by the decision tree (**Figure 2B**). If CO_{MOD} is available, we assign this value as CO_1, and if not, $CO_1 = CO_T$. If CO_{LVOT} is available, we average CO_1 and CO_{LVOT}. Otherwise, CO_1 is taken as the TTE CO for the patient.

For the RHC, there are two CO estimates:

(i)   CO by thermodilution (CO_{Thermo}), and

(ii)   CO calculated via the Fick method (CO_{Fick}).

If CO_{Thermo} is available, it is taken as the patient's CO from RHC. If not, CO_{Fick} is used (**Figure 2C**). **Table 1** lists the data used in this study screened with these decision criteria.

<div align="center">

TABLE 1 – DATA

FIGURE 3 HERE – MODEL SCHEMATIC

FIGURE 4 HERE – MODEL PREDICTIONS

</div>

Mathematical modeling framework

The cardiovascular systems model is similar to that used in a previous study from our lab (Colunga *et al.*, 2020) and is based on the formulation developed by Smith et al. (Smith *et al.*, 2004). **Figure 3** shows the detailed cardiovascular model schematic. The model complexity was reduced significantly since the clinical data used for parameterization here do not have enough informational content to uniquely identify the parameters of the full Smith et al. model. In our previous reduced version of the model, ventricular-ventricular interaction and fluid inertance after each heart valve were omitted. Additionally in this study, the pericardial compartment was removed, and the zero pressure (or dead space) volumes in all vascular and ventricular compartments were set to zero.

Overall, the model used here has 6 states (compartmental blood volumes listed in **Equations (S18)-(S23)** of the Supplemental Material) and 16 parameters each with a specific physiological

interpretation (**Table 2**). Equations for the reduced cardiovascular system model used in this study are given in Section **S1** of the Supplemental Material and model code without parameter optimization can be found at (Carlson *et al*., 2021). Figure **S5** in the Supplemental Material displays the model predictions for normal cardiovascular function corresponding to the parameters listed in Table **S1** of the Supplemental Material. **Figure 4** shows the model predictions for representative HFrEF (panels **A-D**) and HFpEF (panels **E-H**) patients showing the LV and systemic pressures (panels **A** and **E**), RV and pulmonary pressures (panels **B** and **F**), LV and RV volumes (panels **C** and **G**), and pressure-volume loops (panel **D** and **H**). Figures for all model predictions for each patient can be found in **Figures S6-S34** of the Supplemental Material.

TABLE 2 - PARAMETER DESCRIPTIONS

Nominal parameters and initial conditions: Nominal estimates of all parameters are determined starting with the set of expressions from our previous study (Colunga *et al.*, 2020) as a guide. However, some estimated values used in the previous nominal parameter calculations can be replaced with data or calculated directly since TTE measurements are available. Therefore, a reformulation of some nominal parameter expressions has been made in this study:

- LV elastances were calculated from measured volume and estimated pressure in systole.
- LV diastolic stiffness was calculated from measured volume and estimated pressure in diastole.
- RV elastances were calculated from measured pressure and estimated volume in systole.
- RV diastolic stiffness was calculated from measured pressure and estimated volume in diastole.
- Systemic elastances were calculated from measured arterial pulse pressures, estimated venous pulse pressures, and estimated stressed volumes.
- Pulmonary elastances were calculated from estimated and measured pulse pressures and estimated stressed volumes.
- Systemic and pulmonary resistances were calculated from measured systemic and pulmonary average arterial pressures and estimated systolic venous pressure along with the measured RHC CO.

Resistances across the four valves were calculated in exactly the same way as in our previous study, and the ventricular end-diastolic reference pressures were set to normal values from Smith et al. More details on the exact expressions used for nominal calculations are shown in Supplemental Material **S3** and the model code (Carlson *et al*., 2021).

Total blood volume is calculated based on the height, weight, and sex of each patient as described in Colunga et al. (Colunga *et al.*, 2020), utilizing the expression originally developed by Nadler et al. (Nadler *et al.*, 1962). This total blood volume is comprised of stressed and unstressed volumes. The unstressed blood volume is the volume in each compartment at which the pressure is zero. The stressed volume is the difference between the total and unstressed volumes. The initial distribution of stressed and unstressed blood volume among the six vascular compartments is based on the work by Beneken (Beneken & DeWit, 1967), in which a total stressed volume of 18.75% was assumed. In this study, we assumed 30% of the total blood volume is stressed volume (Colunga *et al*., 2020; Maas *et al*., 2012), so additional volume was recruited from the four systemic and pulmonary compartments based on the unstressed volume available in each compartment. Explicit details on determining patient-specific stressed volume for each model compartment can be found in the Supplemental

Material in Section **S4** and the model code (Carlson *et al.*, 2021). In this study, the percent of stressed volume remains the same across all patients. However, regulation of stressed and unstressed volume is a current topic of discussion in the field of HF (Fallick *et al.*, 2011; Fudim *et al.*, 2017), and the ability to change the ratio of stressed and unstressed volume can be explored in future studies.

Global sensitivity analysis: Since the inverse problem investigated here is ill posed, a sensitivity analysis is performed to assess the practical identifiability of the parameters, i.e., determine which of the parameters can be identified with the given clinical patient data. Due to the vast variation in parameter values across subjects, we conducted a global sensitivity analysis using Sobol' indices to explore the entire parameter space. Sobol' indices apportion the variance in the output to the effect of each parameter (Sobol′, 2001). In particular, we use total effect Sobol' indices to characterize the effect of both the parameter and parameter interactions on the residual variance (Randall E. B. *et al.*, 2021). All parameters were varied within their physiological bounds, listed in Table **S1** of the Supplemental Material. The residual (**Equation S80** in the Supplemental Material) was calculated by determining the least square error between simulations and RHC and TTE data in a similar fashion to that described in Colunga et al. (Colunga *et al.*, 2020). The Sobol' indices were calculated using Monte Carlo integration by computing $10^3(16 + 2) = 1.8e4$ model evaluations similar to the procedure described in Randall et al. (Randall E. B. *et al.*, 2021). We then ranked the total effect Sobol' indices (**Figure 7**) to determine a set of influential parameters that substantially affect the variance of the residual, i.e., a subset of parameters that have an index above the threshold $\eta = 10^{-3}$. Parameters below the threshold were excluded from consideration for optimization and set to their nominal values. Though the parameters $P_{0,LV}$, $P_{0,RV}$, and E_{SV} were above η, they are correlated to other parameters with a higher sensitivity and therefore cannot be determined explicitly (Colunga *et al.*, 2020). Hence, $P_{0,LV}$, and $P_{0,RV}$ were set to the values used in Colunga et al., and E_{SV} was calculated using **Equation (S47)** in the Supplemental Material. Note that our previous study used only RHC data to determine model parameters. Since TTE data were included here, two additional model parameters could be identified: E_{LV} and E_{RV}. From the set of influential parameters, we obtained the subset

$$\theta = \{\lambda_{LV}, \lambda_{RV}, E_{LV}, E_{RV}, E_{SA}, E_{PA}, E_{PV}, R_{sys}, R_{pul}\} \tag{3}$$

to optimize. This subset consists of parameters λ_{LV}, λ_{RV}, E_{LV}, and E_{RV}, which are used to describe cardiac function. All others are hemodynamic parameters that define cardiovascular function as a whole, which may be important for distinguishing particular subgroups of HFpEF. This methodology produced a subset of uncorrelated parameters that can be estimated for each patient. In particular, none of the parameters reached their physiological bounds when estimated, giving confidence that the parameter subset in **Equation (3)** is well prescribed to investigate the HF questions discussed here.

Optimization: For each patient, we estimate the adjustable parameters in **Equation (3)** by minimizing the least square error between the simulations and data for ten measurements: RV pressure in systole and diastole, PA pressure in systole and diastole, average PCW pressure, systemic artery pressure in systole and diastole, CO during RHC, LV volume in systole and diastole, and CO during TTE. Since the HR during RHC and TTE can be different, two separate simulations are run: one simulating the RHC and one simulating the TTE. However, both simulations are run with one set of parameter values with the assumption that the parameters representing cardiac function do not change appreciably across procedures for a single patient. Values of the clinical data are calculated over the cardiac cycle after the system has reached a steady state of pulsatile pressures and flows. This is assured by allowing our simulations to run for 50 beats. Once this steady state is reached, the maximum and minimum values of the pressure and volume data of the last 5 beats are used to compute the total residual error. The PCW pressure and CO represent average values over the cardiac

cycle; because of this, their values are averaged over the cardiac cycle before being compared to the TTE and RHC data. Estimates for the adjustable parameters are obtained using the genetic algorithm with a population size of 500 and a stall generation limit of 10 generations implemented in MATLAB (MathWorks Natick, Ma). All other specifications were set to their default MATLAB value. To check to see if the parameter space was explored adequately, we ran the optimization for each patient 10 times and observed a consistent residual across the best few runs. The run with the lowest cost was chosen for our final results. More details about MATLAB's implementation of the genetic algorithm can be found at mathworks.com.

Machine learning

We utilized one classification and two different clustering techniques using the built-in MATLAB k-means and hierarchical clustering functions to group individuals within a population based on similar characteristics. In theory, patients within the same groups should share similar physiological characteristics. The clinical data and optimized parameter values were compiled into separate matrices where each row represents a given patient, and each column represents a clinical measure or optimized parameter value (**Tables 1** and **2**). Before any of the clustering methods are applied, each column is centered by subtracting the average of each column from each element in that column. Because our clinical data and optimized parameters had different units within their respective matrices, we normalized each clinical measure or parameter by its standard deviation. To mitigate any bias in these analyses, no additional weighting is placed on any of the clinical measurements or optimized parameters.

Principal component analysis (PCA): We performed a PCA (Jolliffe IT, 1986), which is simply a singular value decomposition identifying an orthogonal change of basis within the clinical data or optimized parameter spaces that retains the greatest variation across patients, independent of the level of dimension reduction selected. For the optimized parameter matrix P, the decomposition $P = USV^T$ produces unitary matrices U and V and diagonal matrix S, representing the portion of the total variation explained by each principal component. The PCA score, which gives the position in this rotated space that maximizes variation, is given by the product of U and S. **Figure 6A** plots the two-dimensional space of the first two principal components describing more than 50% of the total variance. Subsequent principal components each accounted for less than 15% of the total variance and are not plotted for clarity. A convex hull was prescribed about the HFpEF and HFrEF groups. HFpEF patients are then assigned a group based on the following clustering methods.

k-means clustering: k-means clustering creates k unsupervised clusters from the data. In this study, we chose to group the patients into two clusters, that is, two patients are randomly chosen as cluster centroids, and all other patients are grouped relative to their L_1-distance from each centroid. This method is dependent on the random initial cluster centroids selected, so we run this process 20 times and select the clustering result that has the smallest total cluster variance (Eisen *et al.*, 1998; Wilkin & Huang, 2008). **Figure 4B** shows the two k-means clusters of the clinical data superimposed on the PCA hulls.

Hierarchical clustering: In this clustering method, each patient starts as a cluster, and then the two closest patients are grouped together. This process is repeated, grouping the two closest clusters together to reduce the total number of clusters by 1 until all the patients are in one cluster (Kraskov *et al.*, 2005). This method forms a hierarchical cluster tree known as a dendrogram that can then be truncated to produce the desired number of clusters. To do this in MATLAB, the linkage function is used and the Ward metric (Ward, 1963) is selected to group the two clusters together at each step that minimize the total in-cluster variation. Using the dendrogram, we partitioned our patients into two

clusters by cutting the dendrogram halfway between the second-from-last and last linkages. **Figure 6C** superimposes the hierarchical clusters of the clinical data on the PCA hulls.

Our focus is to identify groups that cluster consistently among these methods, especially since they use different concepts to group the data. If two HFpEF patients share a PCA hull region, a k-means cluster, and a hierarchical cluster, they are included in the same group. Since our purpose here is to subdivide only the HFpEF patients all HFrEF patients are grouped according to their clinical diagnosis independent of whether they may cluster with HFpEF in one of the clustering methods used. The clusters with the most HFrEF patients are considered the most "HFrEF-like". Patients that switch between clusters for different methods are deemed not consistently clustered (NCC).

To classify the HFpEF patients that fall in the PCA overlap region, we rely on the clustering methods. If a HFpEF patient in the overlap region falls in the k-means and hierarchical clusters that contain a majority of the HFrEF patients, we classify them as HFrEF-like HFpEF and thus are part of HFpEF1. Conversely, if they fall in the k-means and hierarchical clusters that contain a majority of HFpEF patients, we classify them as "pure" HFpEF and are part of HFpEF2. If they switch between clusters, they are classified as NCC.

FIGURE 5 - CLINICAL DATA BOX AND WHISKER PLOTS

Results

HF subgroups determined from clinical data

Our retrospective cardiovascular systems analysis consists of a cohort of 31 patient records (10 HFrEF and 21 HFpEF). First, we consider the clinical data explicitly from the RHC and TTE (**Figure 5**). Statistically significant differences in the means of TTE derived measurements (p-value < 0.001) such as EF, systolic & diastolic LV volumes, and CO (p-value < 0.01) are found between HFrEF and HFpEF patients (**Figure 5A-D**). Consistent with their systolic dysfunction phenotype, HFrEF patients have greater ventricular volumes than the HFpEF cohort, with patients 1 and 6 showing particularly extreme ventricular dilation (**Figure 5B** and **C**). In the HFpEF cohort, pulmonary artery systolic and diastolic pressures as well as RV systolic pressures are significantly higher (p-value < 0.01) than the HFrEF cohort (**Figure 5E-G**). Systolic arterial pressure is likewise significantly higher (p-value < 0.05) in the HFpEF cohort when compared to HFrEF patients (**Figure 5H**).

FIGURE 6 - CLUSTERING ANALYSIS WITH CLINICAL DATA

To determine if novel subgroups of HF patients with similar cardiovascular etiologies could be discerned from clinical data alone, we perform a PCA along with two unsupervised clustering methods on the clinical data available from the RHC and TTE (**Figure 6**). All RHC and TTE patient data to which the model was optimized (**Table 1**) except EF, height, and weight were included in the PCA. Since EF was a major factor used to determine clinical diagnosis and LV diastolic and systolic volumes are already included in the PCA analysis, EF was excluded. In **Figure 6A**, PCA scores for the first and second principal components are plotted, and convex hulls are drawn around each diagnosis. The first two principal components of our clinical data PCA describe 52% of the total variance. The convex hulls for HFrEF (orange) and HFpEF (blue) overlap, consisting of HFrEF patients 2, 4, 5, 7, and 9 and HFpEF patients 11, 24, and 18. As PCA only captures the greatest variance across all patients, the HFpEF patients in the overlap region required further analysis.

To test if we could attribute the HFpEF patients that fall in the PCA overlap region into a distinct phenotype associated with the HFrEF or HFpEF clinical groups, we employ k-means and hierarchical clustering (**Figure 6B** and **C**). We superimpose the k-means clusters on the PCA convex hulls (**Figure 6B**). Since all HFrEF patients except patient 5 fall into k-means cluster A, we designate

cluster A as more HFrEF-like and, conversely, k-means cluster B as more HFpEF-like. We observe in the overlap region, HFpEF patient 11 is in k-means cluster A whereas patients 18 and 24 are k-means cluster B. Also, HFrEF patient 5 falls in k-means cluster B. Lastly, HFpEF patients 16, 17, 20, 21, 23, and 27 fall into k-means cluster A. In a similar fashion, hierarchical clustering results are superimposed on the PCA convex hull (**Figure 6C**). Similarly, we specified hierarchical cluster A as more HFrEF-like and hierarchical cluster B as more HFpEF-like. Of particular interest is that all HFpEF patients in the overlap region now fall in hierarchical cluster B.

TABLE 3 – GROUPS FROM CLUSTERING

Among the clustering methods used here, **Table 3** denotes which patients consistently cluster in the following groups:

- "pure" HFrEF ($n = 10$) - patients that fall in the HFrEF PCA hull.
- "pure" HFpEF ($n = 13$) - patients that fall in the HFpEF PCA hull, k-means cluster B, and hierarchical cluster B.
- NCC ($n = 8$) - patients that do not consistently cluster.

Note that this methodology shows no subgroups of HFpEF. Also, almost half of the HFpEF patients fall in the NCC designation. More details of the patient designation based on the clinical measurement clustering analysis are given in **Table S6** in the Supplemental Material.

HFrEF patients 1 and 6 show extreme ventricular dilation compared to other HFrEF patients in this cohort with large systolic and diastolic volumes (outliers in **Figure 5B** and **C**). Therefore, these patients were excluded from further analysis.

FIGURE 7 - GLOBAL SENSITIVITY ANALYSIS RESULTS

HF subgroups determined from optimized parameter values

To learn about the underlying physiological differences between our patient cohorts that cannot be determined from clinical data alone, patient clinical measurements are used to parameterize a simplified cardiovascular systems model. We conduct a global sensitivity analysis exploring the entire permissible parameter space and ranked the parameters due to their contribution to the residual. **Figure 7** displays the ranked total Sobol' indices for all 16 adjustable parameters. This analysis shows that 12 parameters are influential to the residual from which we selected a subset of 9 parameters to optimize (**Equation (3)**).

TABLE 4 - OPTIMIZED PARAMETER VALUES

FIGURE 8 - CLUSTERING ANALYSIS WITH OPTIMIZED PARAMETERS

Our model simulations predict that the HFpEF cohort has a much wider distribution of the parameter values than the HFrEF cohort. We perform the same methods applied to the clinical data to the optimized parameter values to see if in the parameter space we could identify subgroups of HFpEF patients with similar cardiovascular etiologies (**Figure 6**). The first two principal components of our optimized parameter PCA describe 59% of the total variance. Since the clinical data and parameter space are two entirely different representations of the patient population no conclusion should be drawn from the fact that both PCA analyses represent an equivalent total variance for the first two principal components.

The PCA scores of the optimized parameters show that HFpEF patients 11, 17, 18, 29 and 30 fall in the PCA overlap region (**Figure 8A**). We conducted k-means (**Figure 8B**) and hierarchical (**Figure 8C**) clustering on the optimized parameters revealing a much different structure than clustering based

on raw clinical data alone. In both clustering methods, the majority of the HFrEF patients fell into one cluster, which we designate as cluster A (all HFrEF patients except 2 and 9 are in k-means cluster A whereas all HFrEF patients are in hierarchical cluster A). Notably, all HFpEF patients in the overlap region also fall into cluster A for both methods. Therefore, we conclude that this is a distinct HFpEF subpopulation.

Table 3 shows that this independent analysis with PCA, k-means clustering, and hierarchical clustering on the optimized parameter values reveals that the 29 patients fall into distinct groups:

- HFrEF ($n = 8$) - patients that fall in the HFrEF PCA hull.
- HFpEF1 ($n = 5$) - HFpEF patients that fall in the PCA overlap region, k-means cluster A, and hierarchical cluster A.
- HFpEF2 ($n = 11$) - HFpEF patients that fall in the HFpEF PCA hull, k-means cluster B, and hierarchical cluster B.
- NCC ($n = 5$) - HFpEF patients that do not consistently cluster.

Since HFpEF1 shares most of the characteristics of the pure HFrEF group, we consider this group as more HFrEF-like, whereas HFpEF2 is "purely" HFpEF. All of the patients belonging to NCC are HFpEF patients. Additional details about the hull location and clustering for each patient based on the optimized parameter values are shown in **Table S7** of the Supplemental Material.

FIGURE 9 - OPTIMIZED PARAMETER BOX AND WHISKER PLOTS

Analysis of the optimized parameter values from the 4 HF subgroups

Figure 9 illustrates the patient-specific values of key model parameters representing LV active contractility (E_{LV}), LV passive stiffness (λ_{LV}), systemic arterial stiffness (E_{SA}), and systemic (R_{sys}) and pulmonary (R_{pul}) resistance when broken out into the parameter-based HFrEF and HFpEF groups. Parameter values that indicate normal cardiovascular function (listed in Table **S1** of the Supplemental Material) are indicated by the dotted lines, and all parameter values are normalized to these values in **Figure 9**. When comparing E_{LV} **(Figure 9A)**, HFrEF and HFpEF1 tend to be below normal and HFpEF2 and NCC above normal. **(Table 5)**. When compared to both HFrEF and HFpEF1, HFpEF2 (p-value < 0.001) and NCC (p-value < 0.001) show significantly higher E_{LV}. No significant differences were found between HFrEF and HFpEF1, whereas HFpEF2 had a significantly higher E_{LV} when compared to NCC (p-value < 0.05).

When comparing λ_{LV} **(Figure 9B),** all groups have above normal levels when compared to normal **(Table 5)**. Although no significant differences were observed between HFrEF and HFpEF1, both groups have above normal values where λ_{LV} in HFpEF1 is double the normal value. HFpEF2 and NCC have a λ_{LV} almost triple the normal value **(Table 5)**. When compared to both HFrEF and HFpEF1, HFpEF2 shows significantly higher λ_{LV} (p-value < 0.001). NCC has higher λ_{LV} when compared to HFrEF (p-value < 0.001). HFpEF2 had a significantly higher λ_{LV} when compared to NCC (p-value < 0.01).

Looking at E_{SA} **(Figure 9C)**, both HFrEF and HFpEF1 are near normal whereas HFpEF2 and NCC are above normal **(Table 5)**. HFpEF2 shows significantly higher E_{SA} when compared to both HFrEF (p-value < 0.05) and HFpEF1 (p-value < 0.05). No significant differences were observed between HFrEF and HFpEF1. Likewise, no significant differences were observed between NCC and HFpEF2.

Strikingly, R_{sys} **(Figure 9D)** in both HFrEF and NCC are normal, whereas it is decreased in HFpEF1 and increased in HFpEF2 **(Table 5)**. This is the only parameter in which significant differences are observed between HFrEF and HFpEF1 (p-value < 0.01). HFpEF2 shows significantly higher R_{sys}

when compared to HFrEF (p-value < 0.01), HFpEF1 (p-value < 0.001), and NCC (p-value < 0.001). NCC shows significantly higher R_{sys} when compared to HFpEF1 (p-value < 0.05).

Of note, R_{pul} is normal in HFrEF and reduced by almost half in HFpEF1 whereas it is increased in the HFpEF2 and NCC **(Table 5)**. HFpEF2 shows significantly higher levels of R_{pul} when compared to HFrEF (p-value < 0.05), and HFpEF1 (p-value < 0.05) **(Figure 9E)**. No significant differences were observed between HFrEF and HFpEF1. Likewise, no significant differences were observed between NCC and HFpEF2.

These results show that the main cardiac parameters influencing both HFrEF and HFpEF1 are reduced E_{LV} and slightly elevated λ_{LV} **(Figure 9A** and **B** and **Figure S5** in the Supplemental Material)**, indicating that systolic dysfunction is the primary driver for both patient cohorts. Consistent with the classical definition of HFpEF characterized by diastolic dysfunction, our simulations show that HFpEF2 has significantly increased λ_{LV} and E_{LV} at rest **(Figure 9A** and **B)**. When compared to model-based norms, HFpEF2 and NCC show elevated E_{SA} and R_{pul} **(Figure 9C** and **Table 5)**, and HFpEF2 has an elevated R_{sys} **(Figure 9D)**. Strikingly, HFpEF1 shows reduced levels of both R_{pul} and R_{sys}, whereas HFrEF patients show near normal levels of R_{sys}, R_{pul}, and E_{SA} **(Figure 9 C-E** and **Table 5)**.Taken together, these results stress that changes in the systemic and pulmonary vasculature coupled with changes in cardiac function paint a more complete picture of the cardiovascular state of HFpEF patients.

FIGURE 10 - DATA BOX AND WHISKER PLOTS WITH 4 GROUPS

Analysis of the clinical data from the 4 HF subgroups

Using the 4 HF subgroups, we reanalyze the patient RHC and TTE clinical data **(Figure 10)** between groups. The EF between the HF groups reveals very significant differences between all distinct HF subgroups **(Figure 10A)**. The EF in HFpEF1 is still significantly higher (p-value < 0.01) than that of the HFrEF cohort even though they are the most HFrEF-like. As expected, the EF in HFpEF2 and NCC are significantly higher (p-value < 0.001) than the HFrEF cohort. Of note, the different HFpEF groups have an EF above 50%, consistent with their HFpEF diagnosis yet significant differences amongst EF between HFpEF subgroups are observed. Although no significant differences were found between HFpEF2 and NCC, the HFpEF2 and NCC have a significantly higher EF (p-value < 0.05) than HFpEF1.

The HFrEF cohort displays significantly higher LV systolic volumes **(Figure 10B)** when compared with HFpEF2 (p-value < 0.001) and NCC (p-value < 0.001) yet no significant difference is found between HFrEF and HFpEF1. Similar to HFrEF, HFpEF1 shows significantly higher LV systolic volumes than both HFpEF2 (p-value < 0.001) and NCC (p-value < 0.05). NCC shows significantly higher LV systolic volumes when compared to HFpEF2 (p-value < 0.05). LV diastolic volumes show similar results as the LV systolic volumes. No significant differences were found between HFrEF and HFpEF1 **(Figure 10C).** Both HFrEF (p-value < 0.001) and HFpEF1 (p-value < 0.001) show significantly higher diastolic volumes when compared to HFpEF2. NCC has significantly larger diastolic volumes when compared to HFpEF2 (p-value < 0.001). Comparing the TTE CO at rest between groups did not reveal significant differences between HFrEF and HFpEF1 **(Figure 10D)**. NCC has a significantly higher TTE CO at rest when compared to HFrEF (p-value < 0.01) and HFpEF2 (p-value < 0.001) . HFpEF1 had significantly higher values when compared to HFpEF2 (p-value < 0.05.)

RHC pressure measurements revealed that HFpEF2 had significantly higher systolic and diastolic pulmonary arterial pressures when compared to HFrEF(p-value < 0.05.) **(Figure 10E** and **F)**. Likewise, HFpEF2 shows higher systolic RV pressures when compared to HFrEF (p-value < 0.05) **(Figure 10G)**. Systolic arterial pressure in both HFpEF1 and NCC is significantly higher when compared to HFrEF (p-value < 0.05) **(Figure 10H)**.

Overall, analysis of the clinical data with 4 HF subgroups reveals that all patients have higher pressures at rest, with HFpEF2 showing significantly higher pressures when compared to HFrEF. The main distinguishing factor between groups are systolic and diastolic LV volumes where HFrEF and HFpEF1 both have ventricular volume overload, signifying that greater LV volumes could be used as a biomarker for HFrEF-like HFpEF patients.

Discussion

From this analysis of optimized parameter values representing patient-specific cardiovascular mechanics coupled with unsupervised machine learning techniques, we determine distinct HFpEF subgroups that share similar deep mechanistic phenotypes. These groups could not be determined from clinical data alone but reveal that large LV volumes could be used as a biomarker to indicate HFrEF-like HFpEF patients. Our methodology distinguishing HFpEF groups describes not only the functional details of the cardiovascular system for each population but also for each patient in the population. This approach not only considers mechanical function and hemodynamics in the heart but also the pulmonary and systemic vasculature providing a deeper understanding of the cardiovascular state for each population and each patient.

Clustering of HFpEF groups

While HFrEF is characterized by a well-defined phenotype, HFpEF is comprised from a large constellation of changes at the cardiovascular system level. We found that the HFpEF group presented here can be subdivided into 3 subgroups: HFpEF1 described as "HFrEF-like HFpEF", HEpEF2 as "consistent HFpEF", and NCC as "HFpEF patients that are not consistently clustered" (**Figure 8A-C**). Using PCA and clustering techniques to analyze clinical data alone, the same HFpEF distinctions cannot be seen (**Figure 6A-C**), suggesting that key discriminators of HFpEF into distinct phenotypes reside at the mechanistic level revealed only by using our methodology. Simply looking at the underlying mechanistic parameters from our patient-specific modeling (**Figure 9** for groups HFpEF1, HFpEF2, and NCC), we see that the range of values for the HFpEF population is widely heterogeneous. After finding the 2-dimensional reduced space of parameters derived from the patient-specific tuned models that produces the largest variation across patients through PCA, we can see that there are some HFpEF patients that lie in the same region as the HFrEF patients (**Figure 8A).** Extracted physiological parameters, such as E_{LV} and λ_{LV}, are shown to play an important role in describing these distinct patient populations.

HFpEF1 as HFrEF-like HFpEF

In the HFrEF population, we observe elevated λ_{LV}, an observation in accordance with the increased diastolic myocardial stiffness reported in HFrEF patients (Wang *et al.*, 2018). This is coupled with a reduced E_{LV} at rest (**Figure 9A** and **B**). Our observations are consistent with the current understanding of HFrEF, where systolic dysfunction is the main pathological characteristic describing this phenotype (Pinilla-Vera *et al.*, 2019).

In the heterogenous HFpEF population, we surprisingly found that HFpEF1 (HFrEF-like HFpEF) shares the same overall mechanistic parameter trends as the HFrEF group except with lower R_{pul} and R_{sys} (**Table 5**). Patients in the HFpEF1 group have significantly higher EF than HFrEF patients but a significantly lower EF than the other two HFpEF groups (**Figure 10A**). This could be explained by the fact that while both HFrEF and HFpEF1 show systolic and diastolic LV volume overload when compared to HFpEF2 and NCC (**Figure 10B** and **C**). These results suggest a possible biomarker in high LV volumes for HFpEF patients, identifying patients belonging to HFpEF1. Since they share such similar physiological characteristics with the HFrEF cohort, therapeutic strategies currently employed to alleviate systolic dysfunction in HFrEF patients might be employed in HFpEF1 patients.

Likewise, our results indicate that both HFrEF and HFpEF1 patients would benefit from treatments that would improve LV contractility.

HFpEF2 and NCC

HFpEF2, the "pure" HFpEF group, has very high λ_{LV} coupled with increased in E_{LV} at rest (**Figure 9A** and **B, Table 5**). These patients have reduced ventricular filling during diastole, which leads to low systolic volumes (**Figure 10B** and **C**). This phenotype presents a particular challenge in situations such as exercise where the normal physiological response involves the recruitment of increased SV along with an increased HR requiring a rapid ventricular relaxation for proper filling. The elevated ventricular stiffness in this cohort could explain the increased levels of systolic and diastolic pulmonary artery pressure, systolic RV pressure, and systemic arterial pressure observed in the clinical data of these patients (**Figure 10E-H**). The combination of λ_{LV}, E_{SA}, and higher pressures in the pulmonary and systemic vasculature may account for the increased R_{sys} and R_{pul} also observed in this patient cohort (**Figure 9C-E**).

The NCC group was created out of the need to cluster patients that were distinct from HFrEF but did not fall clearly into HFpEF1 or HFpEF2. In falling between two more clearly defined groups, the NCC group may represent a "spectrum" of patients more than a clearly defined subgroup. Perhaps, this is a population of HFpEF undergoing remodeling and given time may decompensate to HFrEF-like HFpEF. Individuals from the NCC group clearly do not behave like individuals from HFrEF or HFpEF1, as they show high λ_{LV} coupled with elevated E_{LV} at rest (**Figure 9A** and **B, Table 5**). Despite this, NCC displays a milder phenotype than that of the "pure" HFpEF2 group. From the clinical data, NCC EF is the highest among the HFpEF groups, with a systolic LV volume similar to HFpEF2 but diastolic LV volumes similar to HFpEF1 (**Figure 10 A-C**).

Possible clinical presentation of HFpEF subgroups

The distinct HFpEF populations found here are consistent with recent studies describing HFpEF as a disparate phenotype. In three of these studies, machine learning methods were used on a variety of clinical and experimental data (Shah, 2019; Cohen *et al.*, 2020*b*; Hahn *et al.*, 2021). In one such study, analysis of RNA sequencing of RV septal endocardial biopsies on control, HFrEF, and HFpEF patients through unsupervised machine learning identified three HFpEF transcriptome subgroups with distinctive pathways and clinical correlations (Hahn *et al.*, 2021). These HFpEF subgroups include:

I. A HFpEF group close to HFrEF showing the worst clinical outcomes when coupled with metabolic dysfunction
II. A HFpEF cohort with smaller hearts and inflammatory and matrix signatures.
III. A heterogeneous phenotype with pronounced HF symptoms and smaller hearts but lower N-terminal-proB-type natriuretic peptide (NT-proBNP) levels.

Patients in Hahn-I had higher LV volumes, perhaps consistent with the ventricular volume overload we observe in both the HFrEF and HFpEF1 patients in our study. The transcriptome of HFpEF Hahn-I is potentially the closest to HFrEF. Patients in Hahn-II were all female and had the smallest LV size. The small LV size seen in these patients is in accordance with the very small LV volumes observed in our HFpEF2 patients, the only group in our study that has a majority of female patients. Likewise, our NCC group could belong to the heterogeneous Hahn-III.

In a second study, Shah *et al.* utilized quantitative echocardiography phenotyping with unsupervised machine learning to identify 3 HFpEF phenogroups with differing clinical and echocardiographic characteristics and outcomes (Shah, 2019):

I. A group with natriuretic peptide deficiency syndrome.
II. A group with extreme cardiometabolic syndrome.
III. A group with right ventricular cardio-abdomino-renal syndrome

One of the characteristics of Shah-II was that it had the most severely impaired cardiac relaxation compared to the other HFpEF groups. Our HFpEF2 group shows very high λ_{LV} and perhaps falls in this same category.

A third study used plasma protein profiling coupled with latent class clustering analysis was performed, identifying 3 HFpEF clinical phenotypes characterized by distinct echocardiographic parameters and large artery stiffness (Cohen *et al.*, 2020*b*):

I.   A group with the least concentric LVs, largest LV cavities, lowest absolute and relative LV wall thickness, lowest LA volumes, lowest values of resistive arterial load (systemic vascular resistance), pulsatile arterial load (total arterial compliance), and large artery stiffness (carotid-femoral pulse wave velocity).

II. A group with a distinct pattern characterized by small concentric LVs with the lowest LV mass among the groups, the largest left atria, the lowest mitral annular tissue velocities, the stiffest large arteries, and the highest pulsatile and resistive arterial load.

III. A group with a distinct pattern of concentric LV hypertrophy with the highest values of LV wall thickness, LV mass, and LV mass indexed for height; this phenogroup also exhibited relatively low values of resistive arterial load but high pulsatile arterial load indexed for body size (total arterial compliance index).

In our study, when compared to the other HFpEF patients, HFpEF1 has the lowest R_{sys}. Hence, HFpEF1 matches Cohen-I. Similarly, HFpEF2 has the highest R_{sys} and E_{SA} and is similar to Cohen-II.

These studies show novel classifications of HFpEF subgroups based on transcriptomic analysis of endomyocardial biopsy obtained through RHC (Hahn *et al.*, 2021), a detailed clinical, laboratory, ECG, and echocardiographic data phenotyping (Shah, 2019), and plasma biomarker profiling (Cohen *et al.*, 2020*b*). These studies point out clinical markers that may describe these novel HFpEF classifications (i.e., NT-proBNP marker, inflammatory signal differences between groups). However, the nature of cardiovascular hemodynamics, its relationship with the pulmonary and systemic vasculature, and the uniqueness of each patient within a group requires a deep phenotyping approach using clinical data to power cardiovascular model-informed machine learning to define HFpEF subgroups. The methodology presented here identifies similar groupings to these three studies using advanced clinical data and in one case endomyocardial biopsies. However, only routine clinical data is needed, making this methodology more amenable in the clinic once validated.

Role of the systemic vasculature in heart failure

The physiological parameters derived from our cardiovascular system model aligns with the understanding that HFrEF patients have reduced E_{LV}, slightly increased E_{SA}, and normal R_{pul} when compared to normal cardiovascular function (**Figure 9**). This alignment of the underlying mechanistic cardiovascular parameters of the model with the conventional wisdom concerning HFrEF suggests that the clinical data used here is sufficient to describe HFrEF. This also gives us confidence in the profile of the deep phenotypes of HFpEF that are revealed here. Our results reveal that that focusing purely on cardiac function may consistently capture the underlying dysfunction in HFrEF but is not a good approach for understanding HFpEF. For example, HFpEF2 patient 20 has increased R_{pul} and R_{sys}, exhibiting large deviations from normal function in the systemic and pulmonary vasculature. Likewise, NCC patient 28 shows increased λ_{LV} and R_{pul} but has similar E_{LV} and E_{SA} to HFrEF. In both patients, addressing the cause for increased resistances in the systemic and pulmonary vasculature may reduce the burden of the heart in HF.

Limitations

In this study, a general HFrEF group was used as the only reference patient population. This methodology determined five HFpEF1 (HFrEF-like HFpEF) patients. Though this is a small cohort of

subjects, this accounts for 25% of the total HFpEF patients in our study. It is of interest to see if this percentage holds with a larger patient cohort in the future. Here, two clustering methods were selected that used different approaches, but we could have used other common unsupervised methods (e.g., mean-shift). The selection of *k*-means and hierarchical clustering in this study was made since these are robust and complementary approaches that can be applied to a wide variety of data sets. Applying a thorough clustering analysis with not just HFpEF and HFrEF phenotypes but other clinical diagnoses such as pulmonary hypertension might provide greater clarity into the physiological differences between groups.

Based on the TTE systolic and diastolic volumes, HFrEF patients 1 and 6 have severe ventricular dilation. Our cardiovascular systems model was unable to account for these large volumes. Hence, making appropriate changes, such as recruiting different stressed volumes for each patient, decreasing ventricular elastance, or implementing a more detailed model, may capture the pathological complexity of these patients. Regardless of future directions taken, the physiological parameters derived from this simple cardiovascular system model can still be useful determinants for HF classification purposes beyond EF.

Conclusions

HFrEF and HFpEF have classically been defined based on ejection fraction. The HFrEF diagnosis itself is much more understood than HFpEF, which is largely heterogeneous. In accordance with other recent studies, we have determined 3 subgroups of HFpEF with our methodological deep phenotyping approach that uses cardiovascular model-informed machine learning: a HFrEF-like HFpEF group, a "pure" HFpEF group, and a group that exhibits characteristics of both. Moreover, our methodology reveals that potential biomarkers for identifying HFpEF-like HFrEF patients are elevated left ventricular systolic and diastolic volumes. However, these biomarker differences necessary to determine HFpEF subgroups could not be distinguished based on the clinical data alone. Ultimately, the combination of mathematical modeling analysis and machine learning techniques provides immense insight into the classifications of HF as a pathology.

Additional information

Supporting information

Additional supporting information may be found online in the Supporting Information section at the end of the article.

Bibliography

Beneken JEW & DeWit B (1967). A physical approach to hemodynamic aspects of the human cardiovascular system. In *Physical Bases of Circulatory Transport: Regulation and Exchange*, pp. 1–45.

Borlaug BA, Chen H, Lin G, Redfield MM, Lewis GD, Semigran MJ, McNulty SE, LeWinter M, Deswal A & Margulies KB (2015). Response to Letter Regarding Article, "Effects of Sildenafil on Ventricular and Vascular Function in Heart Failure With Preserved Ejection Fraction." *Circ Heart Fail* **8,** 840.

Carlson BC & Jones E (2021) HFpEF Phenotyping Simulation Code (Version 1.1) [Computer software] DOI: 10.5281/zenodo.5215892.

Cohen JB, Schrauben SJ, Zhao L, Basso MD, Cvijic ME, Li Z, Yarde M, Wang Z, Bhattacharya PT, Chirinos DA, Prenner S, Zamani P, Seiffert DA, Car BD, Gordon DA, Margulies K, Cappola T & Chirinos JA (2020*a*). Clinical Phenogroups in Heart Failure With Preserved Ejection Fraction. *JACC Heart Fail* **8,** 172–184.

Cohen JB, Schrauben SJ, Zhao L, Basso MD, Cvijic ME, Li Z, Yarde M, Wang Z, Bhattacharya PT, Chirinos DA, Prenner S, Zamani P, Seiffert DA, Car BD, Gordon DA, Margulies K, Cappola T & Chirinos JA (2020*b*). Clinical Phenogroups in Heart Failure With Preserved Ejection Fraction. *JACC: Heart Failure*; DOI: 10.1016/j.jchf.2019.09.009.

Colunga AL, Kim KG, Woodall NP, Dardas TF, Gennari JH, Olufsen MS & Carlson BE (2020). Deep phenotyping of cardiac function in heart transplant patients using cardiovascular system models. *J Physiol* **598,** 3203–3222.

Corral-Acero J et al. (2020). The "Digital Twin" to enable the vision of precision cardiology. *European Heart Journal* **41,** 4556-4564B.

Dunlay SM, Roger VL & Redfield MM (2017). Epidemiology of heart failure with preserved ejection fraction. *Nat Rev Cardiol* **14,** 591–602.

Edelmann F, Wachter R, Schmidt AG, Kraigher-Krainer E, Colantonio C, Kamke W, Duvinage A, Stahrenberg R, Durstewitz K, Löffler M, Düngen H-D, Tschöpe C, Herrmann-Lingen C, Halle M, Hasenfuss G, Gelbrich G, Pieske B & Aldo-DHF Investigators for the (2013). Effect of Spironolactone on Diastolic Function and Exercise Capacity in Patients With Heart Failure With Preserved Ejection Fraction. *JAMA* **309,** 781–791.

Eisen MB, Spellman PT, Brown PO & Botstein D (1998). Cluster analysis and display of genome-wide expression patterns. *PNAS* **95,** 14863–14868.

Fallick C, Sobotka PA & Dunlap ME (2011). Sympathetically mediated changes in capacitance: redistribution of the venous reservoir as a cause of decompensation. *Circ Heart Fail* 4, 669–675.

Fudim M, Hernandez AF & Felker GM (2017). Role of Volume Redistribution in the Congestion of Heart Failure. *Am Heart J* **6,** 1–10.

Guazzi M, Vicenzi M, Arena R & Guazzi MD (2011). Pulmonary Hypertension in Heart Failure With Preserved Ejection Fraction. *Circulation* **124,** 164–174.

Hahn VS, Knutsdottir H, Luo X, Bedi K, Margulies KB, Haldar SM, Stolina M, Yin J, Khakoo AY, Vaishnav J, Bader JS, Kass DA & Sharma K (2021). Myocardial Gene Expression Signatures in Human Heart Failure With Preserved Ejection Fraction. *Circulation* **143,** 120–134.

Hoendermis ES, Liu LCY, Hummel YM, van der Meer P, de Boer RA, Berger RMF, van Veldhuisen DJ & Voors AA (2015). Effects of sildenafil on invasive haemodynamics and exercise capacity in heart failure patients with preserved ejection fraction and pulmonary hypertension: a randomized controlled trial. *Eur Heart J* **36,** 2565–2573.

Hummel SL, DeFranco AC, Skorcz S, Montoye CK & Koelling TM (2009). Recommendation of Low-Salt Diet and Short-term Outcomes in Heart Failure with Preserved Systolic Function. *Am J Med* **122,** 1029–1036.

Jolliffe IT (1986). *Principal Component Analysis*, 2nd Edition. Springer-Verlag, New York.

Kraskov A, Stögbauer H, Andrzejak RG & Grassberger P (2005). Hierarchical clustering using mutual information. *EPL* **70,** 278–284.

Lang RM, Badano LP, Mor-Avi V, Afilalo J, Armstrong A, Ernande L, Flachskampf FA, Foster E, Goldstein SA, Kuznetsova T, Lancellotti P, Muraru D, Picard MH, Rietzschel ER, Rudski L, Spencer KT, Tsang W & Voigt JU (2016). Recommendations for Cardiac Chamber Quantification by Echocardiography in Adults: An Update from the American Society of Echocardiography and the European Association of, Cardiovascular Imaging. *Eur Heart J Cardiovasc Imaging* **17,** 1-39.e14.

Little WC & Zile MR (2012). HFpEF: Cardiovascular Abnormalities Not Just Comorbidities. *Circ Heart Fail* **5,** 669–671.

Liu LCY, Hummel YM, van der Meer P, Berger RMF, Damman K, van Veldhuisen DJ, Voors AA & Hoendermis ES (2017). Effects of sildenafil on cardiac structure and function, cardiopulmonary exercise testing and health-related quality of life measures in heart failure patients with preserved ejection fraction and pulmonary hypertension. *Eur J Heart Fail* **19,** 116–125.

Maas JJ, Pinsky MR, Aarts LP & Jansen JR (2012). Bedside assessment of total systemic vascular compliance, stressed volume, and cardiac function curves in intensive care unit patients. *Anesth Analg* 115, 880–887.

Nadler SB, Hidalgo JU & Bloch T (1962). Prediction of blood volume in normal human adults. *Surgery* **51,** 224–232.

Narang N, Thibodeau JT, Levine BD, Gore MO, Ayers CR, Lange RA, Cigarroa JE, Turer AT, de Lemos JA & McGuire DK (2014). Inaccuracy of Estimated Resting Oxygen Uptake in the Clinical Setting. *Circulation* **129,** 203–210.

Opotowsky AR, Hess E, Maron BA, Brittain EL, Barón AE, Maddox TM, Alshawabkeh LI, Wertheim BM, Xu M, Assad TR, Rich JD, Choudhary G & Tedford RJ (2017). Thermodilution vs Estimated Fick Cardiac Output Measurement in Clinical Practice. *JAMA Cardiol* **2,** 1090–1099.

Owan TE, Hodge DO, Herges RM, Jacobsen SJ, Roger VL & Redfield MM (2006). Trends in Prevalence and Outcome of Heart Failure with Preserved Ejection Fraction. *N Engl J Med* **355,** 251–259.

Pinilla-Vera M, Hahn VS & Kass DA (2019). Leveraging Signaling Pathways to Treat Heart Failure With Reduced Ejection Fraction. *Circ Res* **124,** 1618–1632.

Randall E. B., Randolph N. Z., Alexanderian A. & Olufsen M.S. (2021). Global sensitivity analysis informed model reduction and selection applied to a Valsalva maneuver model.

Redfield MM, Anstrom KJ, Levine JA, Koepp GA, Borlaug BA, Chen HH, LeWinter MM, Joseph SM, Shah SJ, Semigran MJ, Felker GM, Cole RT, Reeves GR, Tedford RJ, Tang WHW, McNulty SE, Velazquez EJ, Shah MR & Braunwald E (2015). Isosorbide Mononitrate in Heart Failure with Preserved Ejection Fraction. *N Engl J Med* **373,** 2314–2324.

Shah SJ (2019). 20th Annual Feigenbaum Lecture: Echocardiography for Precision Medicine—Digital Biopsy to Deconstruct Biology. *J Am Soc Echocardiogr* **32,** 1379-1395.e2.

Smith BW, Chase JG, Nokes RI, Shaw GM & Wake G (2004). Minimal haemodynamic system model including ventricular interaction and valve dynamics. *Med Eng Phys* **26,** 131–139.

Sobol′ IM (2001). Global sensitivity indices for nonlinear mathematical models and their Monte Carlo estimates. *MATH COMPUT SIMULAT* **55,** 271–280.

Solomon SD et al. (2019). Angiotensin–Neprilysin Inhibition in Heart Failure with Preserved Ejection Fraction. *N Engl J Med* **381,** 1609–1620.

Teichholz LE, Kreulen T, Herman M v. & Gorlin R (1976). Problems in echocardiographic volume determinations: Echocardiographic-angiographic correlations in the presence or absence of asynergy. *Am J Cardiol* **37,** 7–11.

Wachtell K, Gerdts E, Palmieri V, Olsen MH, Nieminen MS, Papademetriou V, Boman K, Dahlöf B, Aurigemma GP, Rokkedal JE & Devereux RB (2010). In-treatment midwall and endocardial fractional shortening predict cardiovascular outcome in hypertensive patients with preserved baseline systolic ventricular function: the Losartan Intervention For Endpoint reduction study. *J Hypertens* **28,** 1541–1546.

Wang ZJ, Wang VY, Bradley CP, Nash MP, Young AA & Cao JJ (2018). Left Ventricular Diastolic Myocardial Stiffness and End-Diastolic Myofibre Stress in Human Heart Failure Using Personalised Biomechanical Analysis. *Journal of Cardiovascular Translational Research* **11,** 346–356.

Ward JH (1963). Hierarchical Grouping to Optimize an Objective Function. *J Am Stat Assoc* **58,** 236–244.

Wilkin GA & Huang X (2008). A practical comparison of two K-Means clustering algorithms. *BMC Bioinformatics* **9,** S19-undefined.

Yancy CW et al. (2013). 2013 ACCF/AHA Guideline for the Management of Heart Failure. *Circulation* **128,** 240–327.

Yancy CW, Jessup M, Bozkurt B, Butler J, Casey DE, Colvin MM, Drazner MH, Filippatos GS, Fonarow GC, Givertz MM, Hollenberg SM, Lindenfeld J, Masoudi FA, McBride PE, Peterson PN, Stevenson LW & Westlake C (2017). 2017 ACC/AHA/HFSA Focused Update of the 2013 ACCF/AHA Guideline for the Management of Heart Failure. *Journal of the American College of Cardiology* **70,** 776–803.

Yancy CW, Lopatin M, Stevenson LW, de Marco T & Fonarow GC (2006). Clinical Presentation, Management, and In-Hospital Outcomes of Patients Admitted With Acute Decompensated Heart Failure With Preserved Systolic Function. *J Am Coll Cardiol* **47,** 76–84.

Yusuf S, Pfeffer MA, Swedberg K, Granger CB, Held P, McMurray JJ, Michelson EL, Olofsson B & Östergren J (2003). Effects of candesartan in patients with chronic heart failure and preserved left-ventricular ejection fraction: the CHARM-Preserved Trial. *The Lancet* **362,** 777–781.

Tables

Table 1: Right heart catheterization (RHC) data, transthoracic echocardiogram (TTE) data, and patient biometrics.

Patient		P_{RV} Sys	P_{RV} Dias	P_{PA} Sys	P_{PA} Dias	$\bar{P}_{PCW}$	P_{SA} Sys	P_{SA} Dias	CO_{RHC}	HR_{RHC}	V_{LV} Sys	V_{LV} Dias	HR_{TTE}	CO_{TTE}	BW	Height	Sex
				RHC Data								**TTE Data**				**Patient Biometrics**	
1		43	3	45	29	24	101	70	5.2	88	250.6	337.5	87	2.9	90.8	175.1	M
2		65	9	69	24	26	113	81	3.6	84	116.3	169.3	100	3.1	90.3	167.8	M
3		21	5	20	11	13	70	45	3.2	68	106.5	115	74	3.2	46.3	162.6	F
4		50	7	42	26	24	109	60	3.7	66	87.9	147.5	76	4.1	91.9	157.2	F
5	HFrEF	45	13	44	22	29	155	98	5.4	68	57.38	202.4	72	4.5	86.2	182.9	M
6		28	1	30	11	11	81	50	3.9	60	231.9	303.3	68	2.1	56.7	162.6	F
7		48	7	47	24	19	149	61	5.5	72	92.2	179.52	70	5.5	112.5	182.9	M
8		25	4	26	13	8	96	66	5.6	69	35.8	99.1	84	3.1	78.4	158	F
9		51	30	52	8	25	116	70	3	82	107	127.7	84	8.1	67.3	183	M
10		41	6	43	22	22	83	60	3.4	78	153.2	162.4	98	3.3	98.1	177	M
Mean		41.7	8.5	41.8	17	20.1	107.3	66.1	4.2	73.4	123.9	184.4	81.3	4	81.9	170.9	
Median		44	6.5	43.5	17.5	23	105	63.7	3.8	70.2	106.8	165.9	80	3.3	88.3	171.5	
SD		12.8	7.8	13.2	6.8	6.7	26.3	14.5	1	8.7	66.1	74.4	10.7	1.6	19	10	
11		46	10	44	20	19	159.5	65.5	6.1	58	99	210	67	5	109.3	158.7	F
12		76	13	69	31	19	108	71.5	5.8	60	51.2	83	70	4.6	106.6	177.9	M
13		53	8	54	24	28	158	64.5	6.84	76	44	107.2	74	4.7	107.5	160	F
14		86	25	89	53	28	165.5	91.5	5.7	64	24.5	92.2	66	4.5	139.7	173	M
15		56	9	53	31	27	146	72	6.1	65	34.9	112.5	70	5.4	101.2	165.1	F
16		45	3	45	20	19	165	69	4.4	63	21.5	57.1	64	3.9	59.4	162.8	F
17		66	6	66	31	29	111	58	3.5	66	65.7	135	69	4.8	136.2	168.3	M
18		42	13	42	23	25	119	76	7.43	101	54.3	159.6	66	4.3	98	166.3	F
19		65	17	65	33	78	164	91	5.67	68	31.9	100.9	73	3.2	125.7	157.3	F
20		88	7	87	25	8	134	60	3.5	53	23.9	49.8	50	3.4	63	160	F
21	HFpEF	37	2	37	18	18	123	63	3.37	67	20.1	58	67	4.6	68.1	171.4	M
22		72	8	72	28	28	157.5	71.5	5.63	71	24.5	117.9	85	5.1	105.3	160	F
23		31	5	33	15	14	136	57	4.5	59	22.1	146.7	67	4.9	62.4	163	F
24		45	11	40	22	14	119	73	6.23	78	22.1	62.8	88	6.1	110.4	166	F
25		104	13	104	39	37	143	82	3.67	75	24.6	96.4	88	4.2	78.9	169	M
26		63	18	65	32	30	121.5	69.5	3.47	58	11.8	58.8	70	4.2	80.5	157	F
27		56	0	53	21	13	105	55	2.9	53	19.9	70.9	55	3.6	60.2	154	M
28		60	10	59	31	17	118	81	4.03	77	34.9	97.1	85	5.3	102.4	168	M
29		73	12	73	19	29	104	60	7.27	65	69.8	147	64	4.9	106.7	175	M
30		65	19	65	34	34	65	34	5.25	80	28.4	77.3	85	4.3	68.8	165	M
31		50	9	49	24	26	156	81	7.53	85	27	70	81	6.7	89.4	159	F
Mean		60.9	10.4	60.2	27.3	25.7	132.3	68.9	5.2	68.6	36	100.5	71.6	4.7	94.3	164.6	
Median		60	10	59	25	26	134	69.5	5.6	66	27	96.4	70	4.6	101.2	165	
SD		17.7	5.9	17.9	8.4	13.8	25.8	12.8	1.4	11.3	20.7	40	10.2	0.8	24.1	6.2	

HFrEF – heart failure with reduced ejection fraction. HFpEF – heart failure with preserved ejection fraction.

P – pressure. V – volume. CO – cardiac output. HR – heart rate. BW – body weight. Sys – systole. Dias – diastole.

Subscripts: LV – left ventricle. RV – right ventricle. PA – pulmonary arteries. PCW – pulmonary capillary wedge. SA – systemic arteries.
Bar notation indicates an average pressure.

Table 2: Model parameters for patients at rest.

Parameter		Units	Description	Fixed	Adjustable
Left Ventricle (LV)	E_{LV}	mmHg mL^{-1}	LV active contractility		X
	$P_{0,LV}$	mmHg	LV diastolic reference pressure	X	
	λ_{LV}	mL^{-1}	LV passive stiffness		X
Right Ventricle (RV)	E_{RV}	mmHg mL^{-1}	RV active contractility		X
	$P_{0,RV}$	mmHg	RV diastolic reference pressure	X	
	λ_{RV}	mL^{-1}	RV passive stiffness		X
Pulmonary Vasculature	E_{PA}	mmHg mL^{-1}	Pulmonary arterial (PA) stiffness		X
	E_{PV}	mmHg mL^{-1}	Pulmonary venous (PV) stiffness		X
	R_{pul}	mmHg s mL^{-1}	Pulmonary resistance		X
Systemic Vasculature	E_{SA}	mmHg mL^{-1}	Systemic arterial (SA) stiffness		X
	E_{SV}	mmHg mL^{-1}	Systemic venous (SV) stiffness	X	
	R_{sys}	mmHg s mL^{-1}	Systemic resistance		X
Heart Valves	R_{mval}	mmHg s mL^{-1}	Mitral valve resistance	X	
	R_{aval}	mmHg s mL^{-1}	Aortic valve resistance	X	
	R_{tval}	mmHg s mL^{-1}	Tricuspid valve resistance	X	
	R_{pval}	mmHg s mL^{-1}	Pulmonary valve resistance	X	

Table 3: Patient classification from clustering results based on clinical data (left) and optimized parameters (right).

Clinical data			Optimized parameters			
HFrEF	HFpEF	NCC	HFrEF	HFpEF1	HFpEF2	NCC
1	12	11	2	11	12	13
2	13	16	3	17	14	15
3	14	17	4	18	16	22
4	15	18	5	29	19	23
5	19	20	7	30	20	28
6	22	21	8		21	
7	24	23	9		24	
8	25	27	10		25	
9	26				26	
10	28				27	
	29				31	
	30					
	31					

HFrEF – heart failure with reduced ejection fraction.
HFpEF – heart failure with preserved ejection fraction.
NCC – not consistently clustered.

23

Table 4: Patient-specific optimized parameter values.

Patient		E_{LV}	λ_{LV}	E_{RV}	λ_{RV}	E_{PA}	E_{PV}	R_{pul}	E_{SA}	R_{sys}
HFrEF	2	1.09	0.04	4.09	0.07	2.18	0.09	0.24	0.93	1.53
	3	0.78	0.03	0.37	0.03	0.70	0.07	0.02	0.67	1.03
	4	1.33	0.04	2.49	0.05	0.40	0.06	0.14	1.09	1.21
	5	1.96	0.03	0.76	0.03	2.99	0.10	0.03	0.88	1.25
	7	1.63	0.03	0.37	0.02	0.46	0.02	0.11	1.49	1.05
	8	2.88	0.04	0.48	0.01	0.24	0.01	0.17	0.54	1.05
	9	1.15	0.04	1.14	0.05	2.61	0.09	0.19	1.84	1.92
	10	0.65	0.03	0.36	0.01	0.73	0.02	0.11	0.68	1.37
	Mean	1.44	0.04	1.26	0.03	1.29	0.06	0.13	1.02	1.30
	Median	1.24	0.04	0.62	0.03	0.72	0.07	0.13	0.91	1.23
	SD	0.68	0.00	1.27	0.02	1.04	0.03	0.07	0.42	0.29
HFpEF1	11	1.73	0.03	2.98	0.03	0.49	0.03	0.06	1.14	0.94
	17	1.77	0.04	1.39	0.02	2.12	0.02	0.08	0.97	1.04
	18	1.52	0.03	0.45	0.02	0.62	0.08	0.03	0.75	0.72
	29	1.49	0.04	1.57	0.03	2.74	0.09	0.11	0.71	0.85
	30	2.39	0.07	1.43	0.01	1.19	0.04	0.11	0.89	0.69
	Mean	1.78	0.04	1.56	0.02	1.43	0.05	0.08	0.89	0.85
	Median	1.73	0.04	1.43	0.02	1.19	0.04	0.08	0.89	0.85
	SD	0.32	0.02	0.81	0.01	0.87	0.03	0.03	0.15	0.13
HFpEF2	12	2.55	0.06	1.77	0.05	1.29	0.05	0.74	1.02	1.90
	14	6.84	0.06	1.31	0.03	0.65	0.10	0.59	1.36	1.50
	16	8.65	0.09	2.16	0.05	0.89	0.02	0.29	3.16	2.70
	19	5.38	0.06	1.09	0.03	1.11	0.10	0.05	1.34	1.39
	20	7.67	0.08	2.00	0.04	1.75	0.03	1.00	2.07	2.13
	21	6.11	0.09	1.01	0.03	0.73	0.02	0.17	2.01	2.11
	24	5.77	0.07	1.20	0.05	0.60	0.10	0.30	1.33	1.51
	25	5.63	0.07	3.13	0.05	2.18	0.10	0.29	1.38	1.39
	26	9.99	0.09	3.40	0.06	0.88	0.10	0.32	1.29	1.72
	27	5.60	0.06	2.21	0.01	0.77	0.01	0.45	1.15	1.67
	31	5.68	0.08	3.19	0.07	1.90	0.03	0.08	2.26	1.81
	Mean	6.35	0.07	2.04	0.04	1.16	0.06	0.39	1.67	1.80
	Median	5.77	0.07	2.00	0.05	0.89	0.05	0.30	1.36	1.72
	SD	1.85	0.01	0.84	0.02	0.52	0.04	0.27	0.61	0.38
NCC	13	3.58	0.05	0.07	0.10	0.91	0.04	0.11	1.97	1.18
	15	4.30	0.05	2.74	0.04	0.42	0.05	0.14	1.21	1.12
	22	6.69	0.05	3.26	0.04	0.89	0.04	0.15	1.36	1.02
	23	6.32	0.04	0.62	0.02	0.26	0.03	0.09	1.08	0.95
	28	3.40	0.06	4.48	0.06	0.74	0.10	0.44	0.86	1.34
	Mean	4.86	0.05	2.23	0.05	0.64	0.05	0.19	1.30	1.12
	Median	4.30	0.05	2.74	0.04	0.74	0.04	0.14	1.21	1.12
	SD	1.38	0.00	1.65	0.03	0.26	0.03	0.13	0.38	0.13

HFrEF – heart failure with reduced ejection fraction.
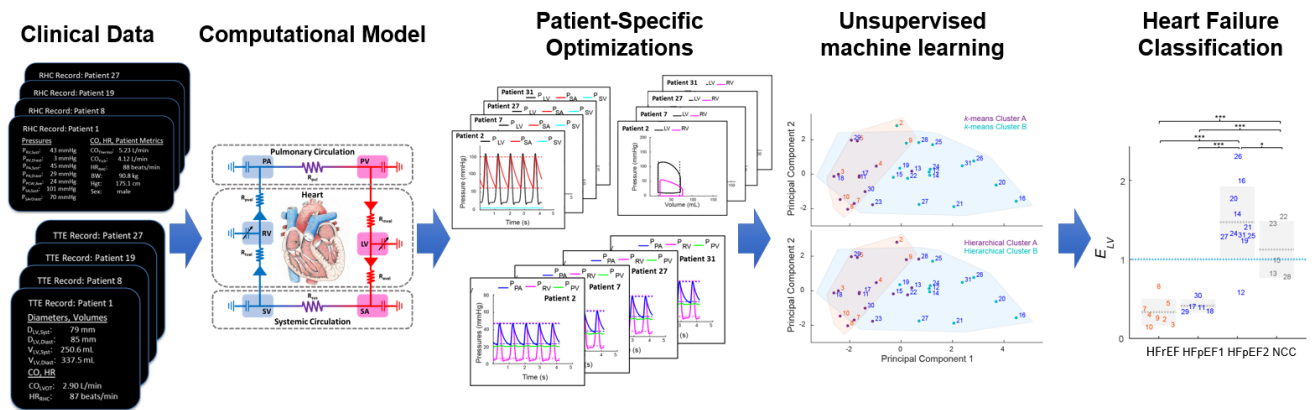HFpEF – heart failure with preserved ejection fraction.
NCC – not consistently clustered.

24

Table 5: Subgroup optimized parameter mean values compared to model-based norms listed in Table **S1** of the Supplemental Material.

Subgroup	E_{LV}	λ_{LV}	E_{RV}	λ_{RV}	E_{PA}	E_{PV}	R_{pul}	E_{SA}	R_{sys}
HFrEF	0.3	1.7	1.8	1.7	5.0	5.7	1.0	1.1	1.0
HFpEF1	0.4	2.1	2.2	1.2	5.5	5.2	0.6	1.0	0.7
HFpEF2	1.5	3.6	2.9	2.1	4.5	5.9	3.0	1.9	1.4
NCC	1.1	2.5	3.2	2.6	2.5	5.0	1.4	1.4	0.9

HFrEF – heart failure with reduced ejection fraction.
HFpEF – heart failure with preserved ejection fraction.
NCC – not consistently clustered.

Figures

Figure 1. Methodology. This schematic shows the workflow analyzing clinical data from right heart catheterization (RHC) and transthoracic echocardiography (TTE) from patients with heart failure with preserved (HFpEF) and reduced (HFrEF) ejection fraction using a patient-specific cardiovascular systems model. A subset of model parameters is optimized to RHC and TTE data for each patient. These parameter values can then be used to observe differences between HFpEF and HFrEF patients and determine subgroups of HFpEF using unsupervised machine learning.
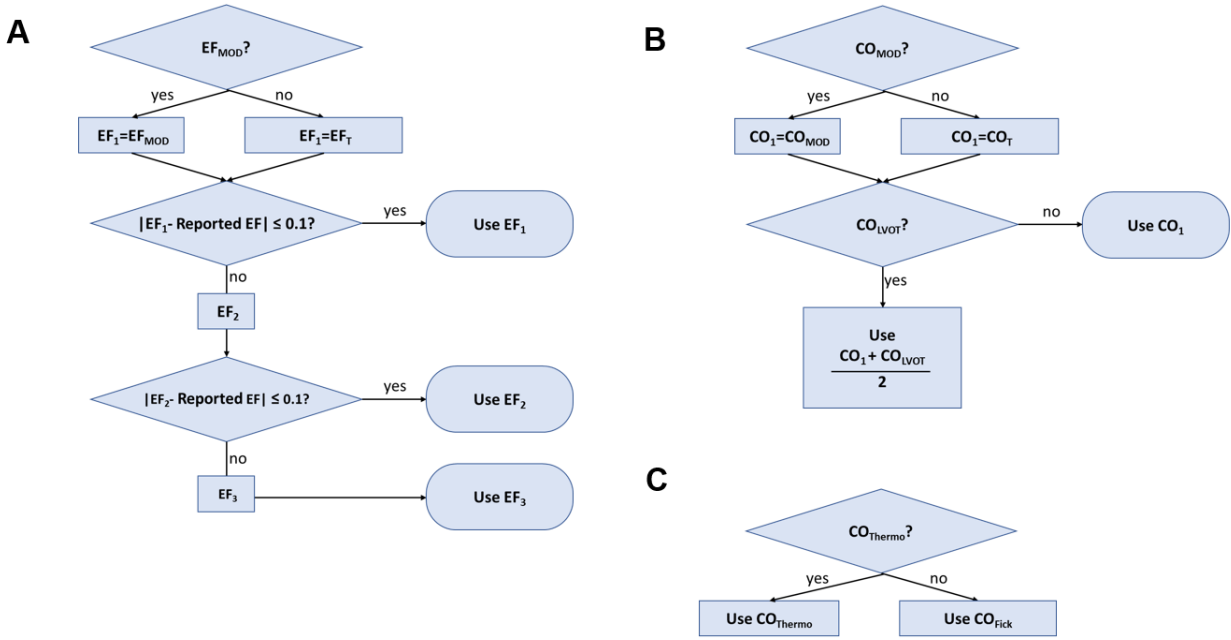
Figure 2. Decision trees. These trees are used to determine which calculation of ejection fraction (EF) and cardiac output (CO) should be used in the right heart catheterization (RHC) and transthoracic echocardiography (TTE) data. **A.** EF from TTE data. This decision tree is used to resolve discrepancies between the reported EF in TTE records and those calculated by Method of Discs (MOD) and Teichholz's formula (EF_T). The result is set to EF_1. EF_2 and EF_3 are calculated using **Equations (1)** and **(2)**, respectively. **B**. CO from TTE data. An estimate of CO from left ventricular (LV) volumes in systole and diastole through the MOD (CO_{MOD}) is our first choice. If CO_{MOD} is not available, CO estimates are calculated from LV diameter data during systole and diastole using Teichholz's formula (CO_T). The result is set as CO_1. If a left ventricular out track flow velocity time integral (LVOT VTI) CO estimate (CO_{LVOT}) is also available, CO_{LVOT} is averaged with CO_1. **C.** CO from RHC data. CO determined via thermodilution (CO_{Thermo}) takes precedence over CO calculated using the Fick method (CO_{Fick}).
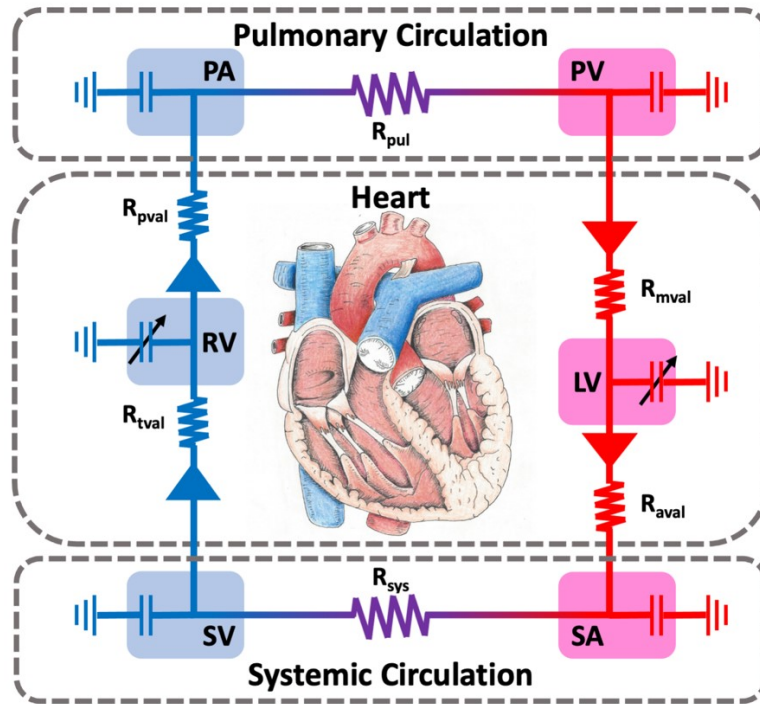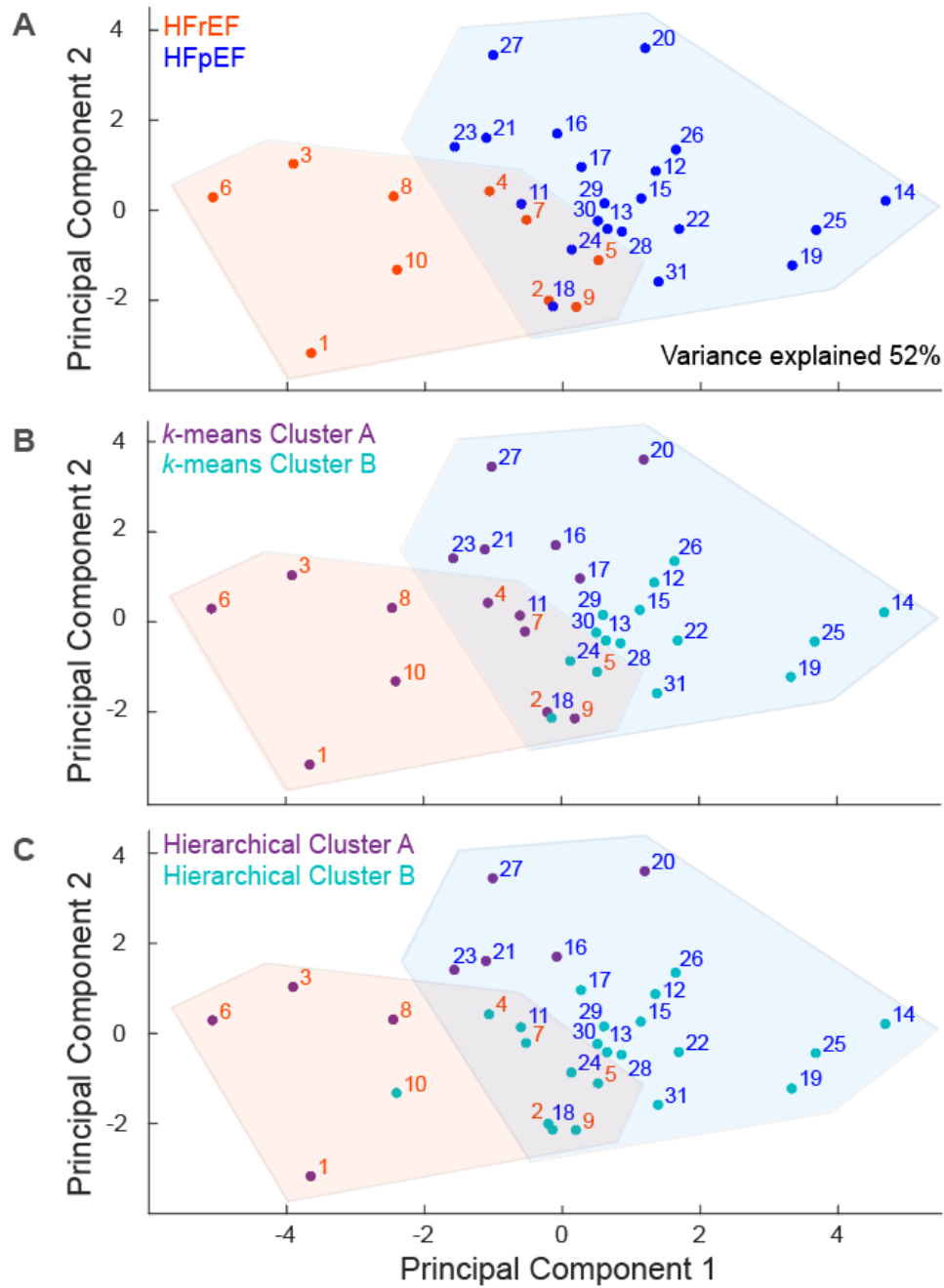
Figure 3. Model schematic. The cardiovascular system model is described using an electrical circuit analogy where pressure, volume, and flow correspond to voltage, charge, and current, respectively. There are 6 compartments (clockwise): left ventricle (LV), systemic arteries (SA), systemic veins (SV), right ventricle (RV), pulmonary arteries (PA), and pulmonary veins (PV). The model has a systemic (R_{sys}) and pulmonary (R_{pul}) resistance denoting the drop in pressure from the arterial to venous compartments. Heart valves are simulated as diodes (triangles) with an associated resistance: mitral valve (R_{mval}), aortic valve (R_{aval}), tricuspid valve (R_{tval}), and pulmonary valve (R_{pval}).
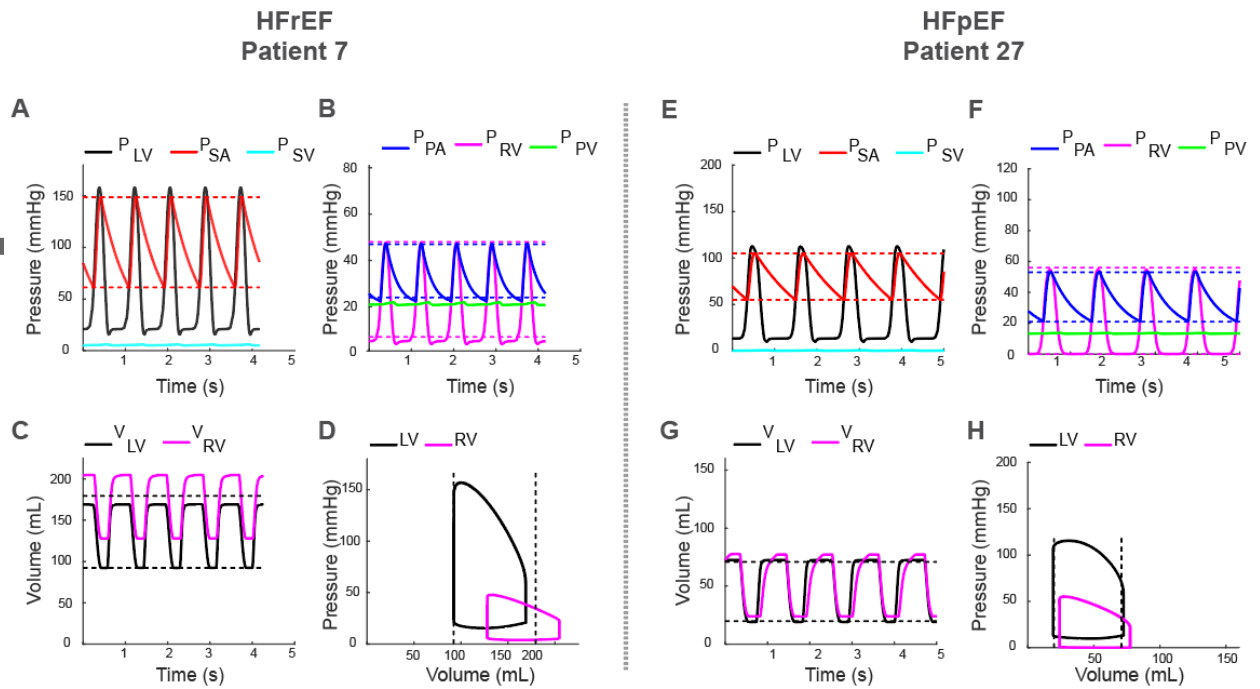
Figure 4. Model predictions. The model predicted pressures and volumes for a representative HFrEF (Patient 7, panels **A-D**) and HFpEF (Patient 27, panels **E-H**) are plotted. **A** and **E**. Pressure (mmHg) time courses for the left ventricle (P_{LV}, black), systemic arteries (P_{SA}, red), and systemic veins (P_{SV}, cyan). Data for the systolic and diastolic systemic arterial pressures are plotted as horizontal dashed red lines. **B** and **F**. Pressure time courses for the right ventricle (P_{RV}, magenta), pulmonary arteries (P_{PA}, blue), and pulmonary veins (P_{PV}, green). Data for the systolic and diastolic right ventricular and pulmonary arterial pressures are plotted as horizontal dashed magenta and blue lines, respectively. **C** and **G**. Volume (mL) time courses for the left (V_{LV}, black) and right (V_{RV}, magenta) ventricles. Data for the systolic and diastolic left ventricular volumes are plotted as horizontal dashed black lines. **D** and **H**. Pressure-volume loops for the left (black) and right (magenta) ventricles. Data for the systolic and diastolic left ventricular volumes are plotted as vertical dashed black lines.
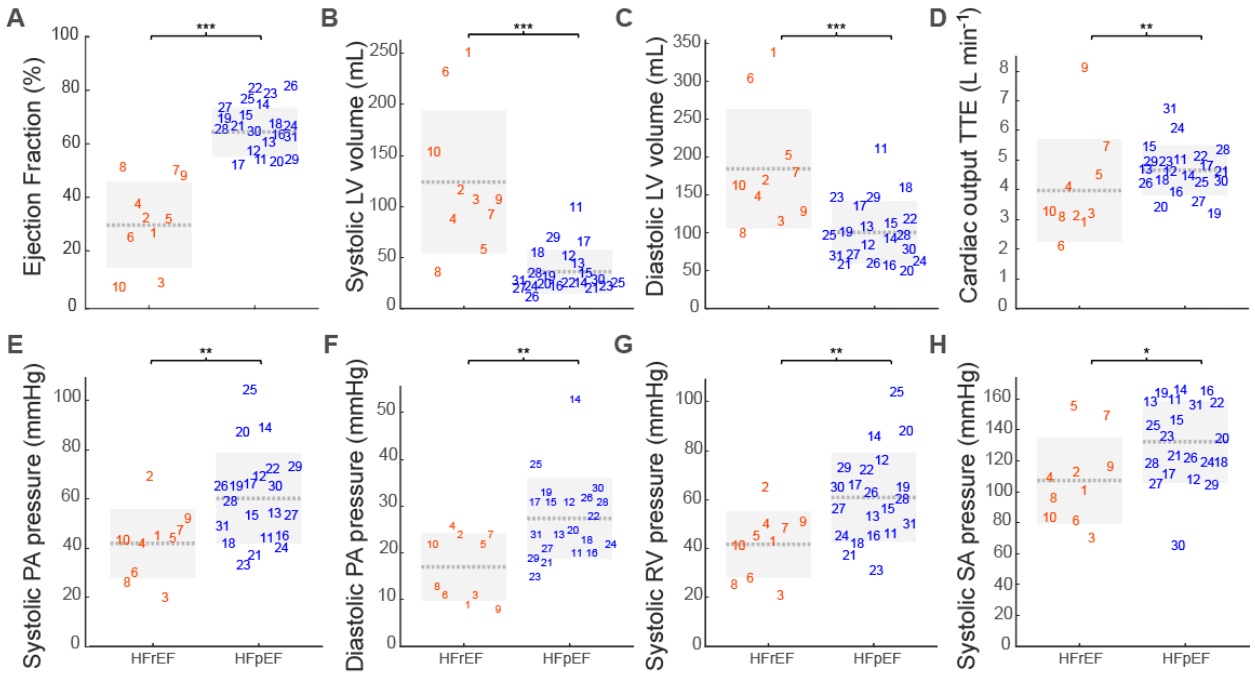
Figure 5. Box plots of clinical data with significant differences between heart failure patients based on their HFrEF and HFpEF diagnosis. **A.** Ejection fraction (%). **B.** Systolic left ventricular (LV) volume (mL). **C.** Diastolic LV volume (mL). **D.** Cardiac output (L min^{-1}) from the TTE data. **E.** Systolic pulmonary arterial (PA) pressure (mmHg). **F.** Diastolic PA pressure (mmHg). **G.** Systolic right ventricular (RV) pressure (mmHg). **H.** Systolic systemic arterial (SA) pressure (mmHg). The light gray dashed line denotes the group average, and the grey box contains one standard deviation above and below the mean of each clinical value (*p-value <0.05, **p-value <.01, ***p-value <.001).
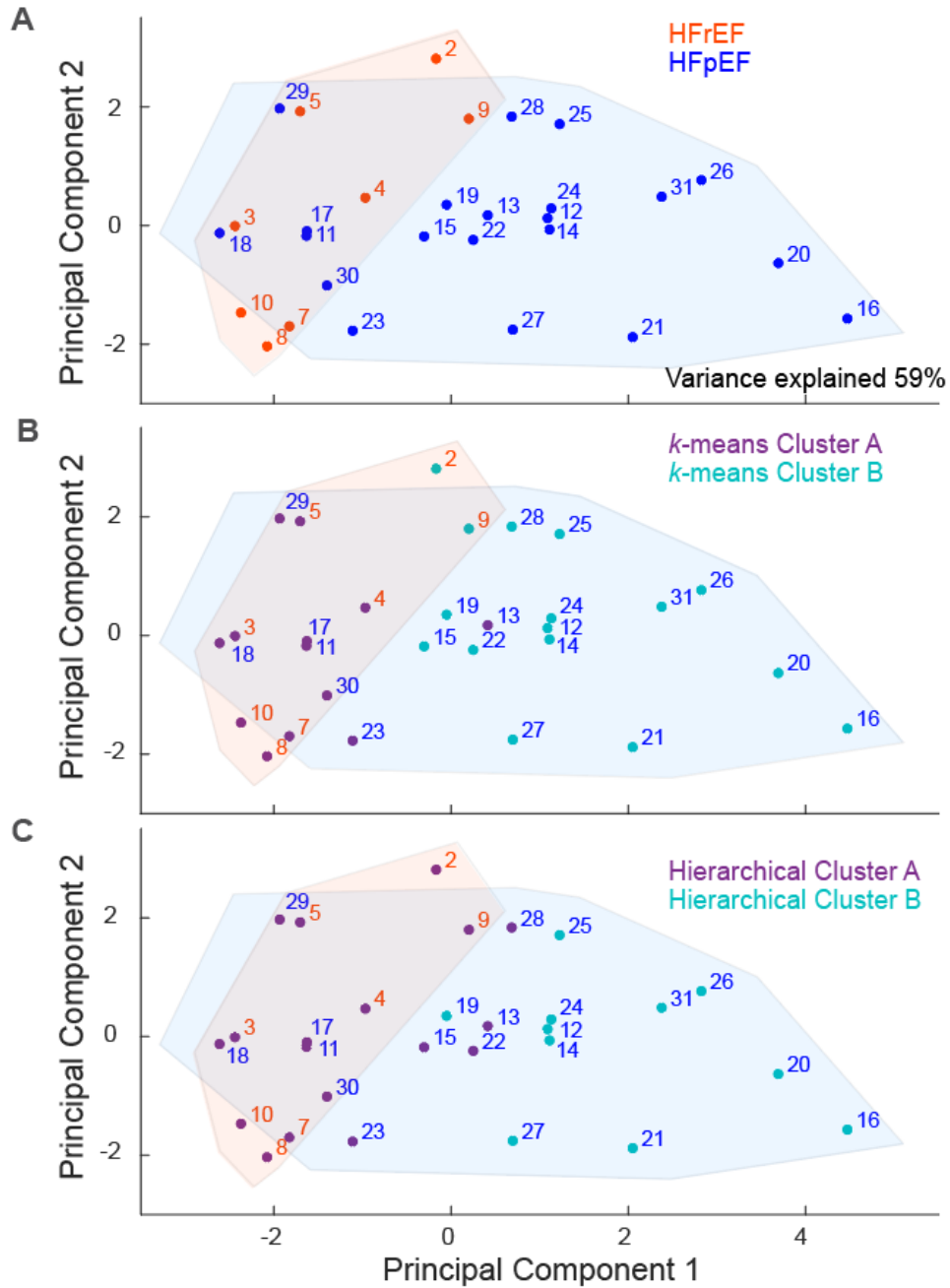
Figure 6. Clustering analysis of clinical data. **A.** Principal component analysis (PCA) of the clinical data. Convex hulls for the HFrEF (orange) and HFpEF (blue) patients are determined by individual patient diagnosis. **B.** k-means clustering of patient data superimposed on the PCA hulls where cluster A (purple) is more HFrEF-like and cluster B (teal) is more HFpEF-like. **C.** Hierarchical clustering of patient data superimposed on the PCA hulls where cluster A (purple) is more HFrEF-like and cluster B (teal) is more HFpEF-like.
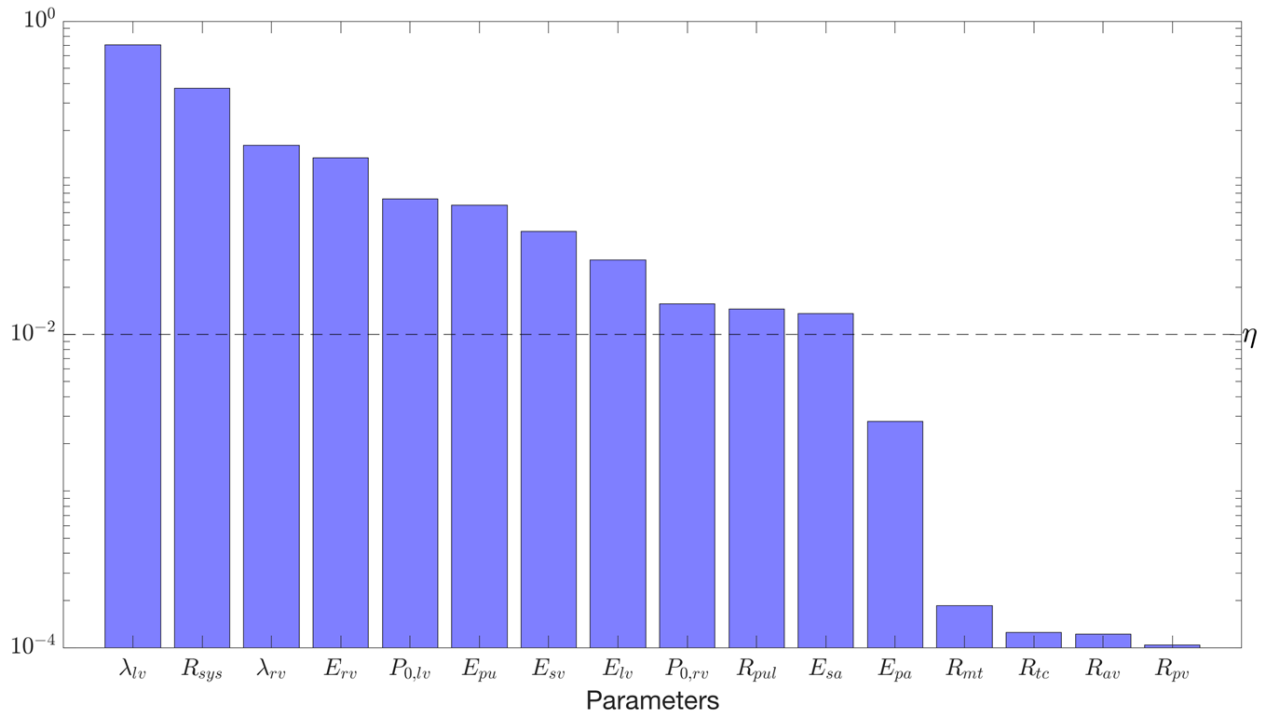
Figure 7. Global sensitivity analysis. Ranked total Sobol' indices for all 16 adjustable parameters with an index above the threshold $\eta = 10^{-2}$ were plotted with a log-scaled y-axis. This analysis shows that 12 parameters are influential to changes in the residual. From these parameters, we selected a subset of parameters to optimize, given in **Equation (3)**.

Figure 8. Clustering analysis of optimized model parameter values. This analysis determines three distinct groups of HFpEF patients. **A.** Principal component analysis (PCA) of the optimized model parameters. Convex hulls for the HFrEF (orange) and HFpEF (blue) patients are determined by individual patient diagnosis. **B.** *k*-means clustering of optimized parameter values superimposed on the PCA hulls where cluster A (purple) is more HFrEF-like and cluster B (teal) is more HFpEF-like. **C.** Hierarchical clustering of optimized parameter values superimposed on the PCA hulls where cluster A (purple) is more HFrEF-like and cluster B (teal) is more HFpEF-like.
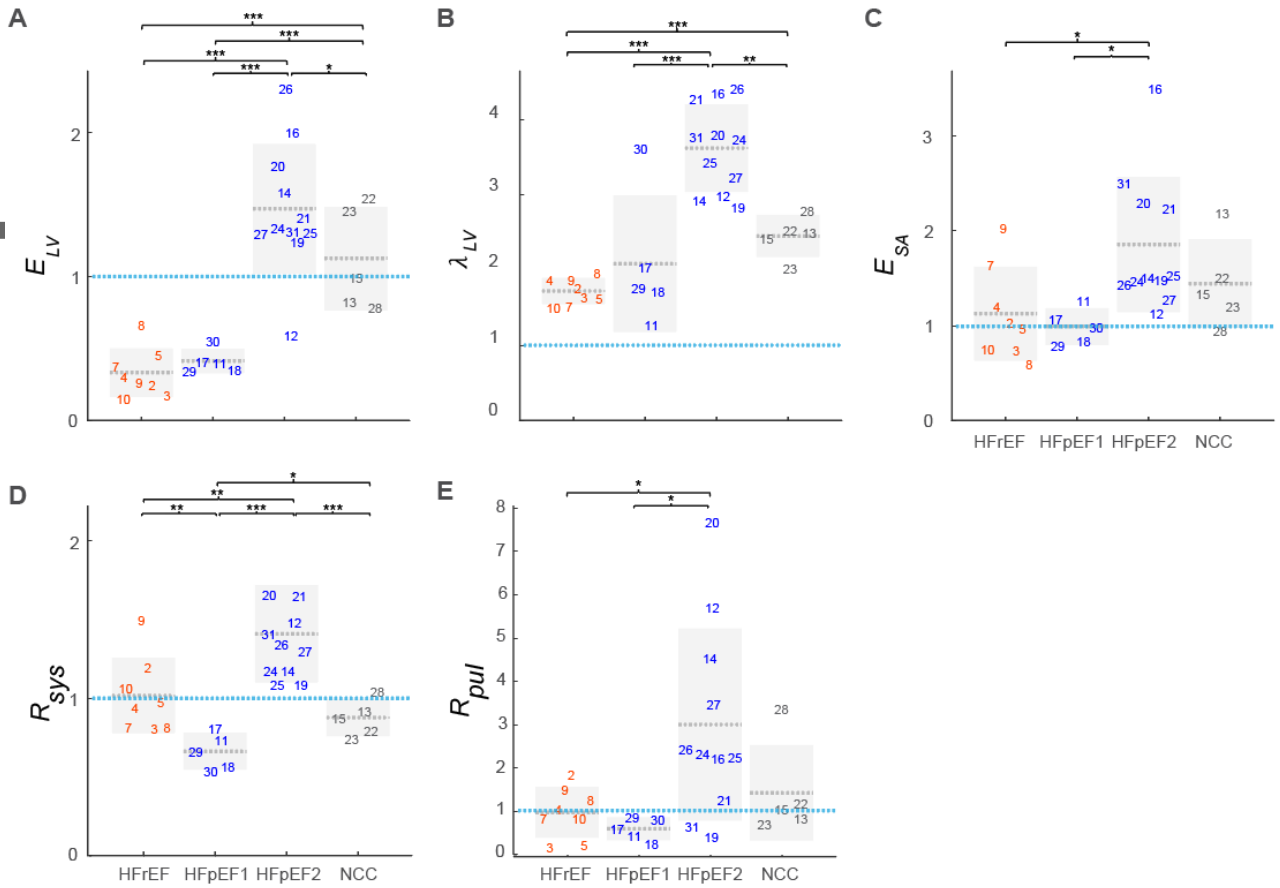
Figure 9. Box plots of the optimized parameter values with 4 heart failure groups. Analysis of the optimized parameters gives us an understanding of the mechanistic differences between the three HFpEF groups that cannot be seen by analyzing the clinical data alone. **A.** Left ventricular (LV) active contractility (E_{LV}, mmHg mL^{-1}). **B.** LV passive stiffness (λ_{LV}, mL^{-1}). **C.** Systemic arterial (SA) stiffness (E_{SA}, mmHg mL^{-1}). **D**. Systemic resistance (R_{sys}, mmHg s mL^{-1}). **E.** Pulmonary resistance (R_{pul}, mmHg s mL^{-1}). All values are plotted relative to the normal model values given in Table **S1** of the Supplemental Material, indicated by the horizontal dashed blue line. The light gray dashed line denotes the average, and the gray box contains one standard deviation above and below the mean of each parameter value (*p-value <0.05, **p-value <0.01, ***p-value <0.001).
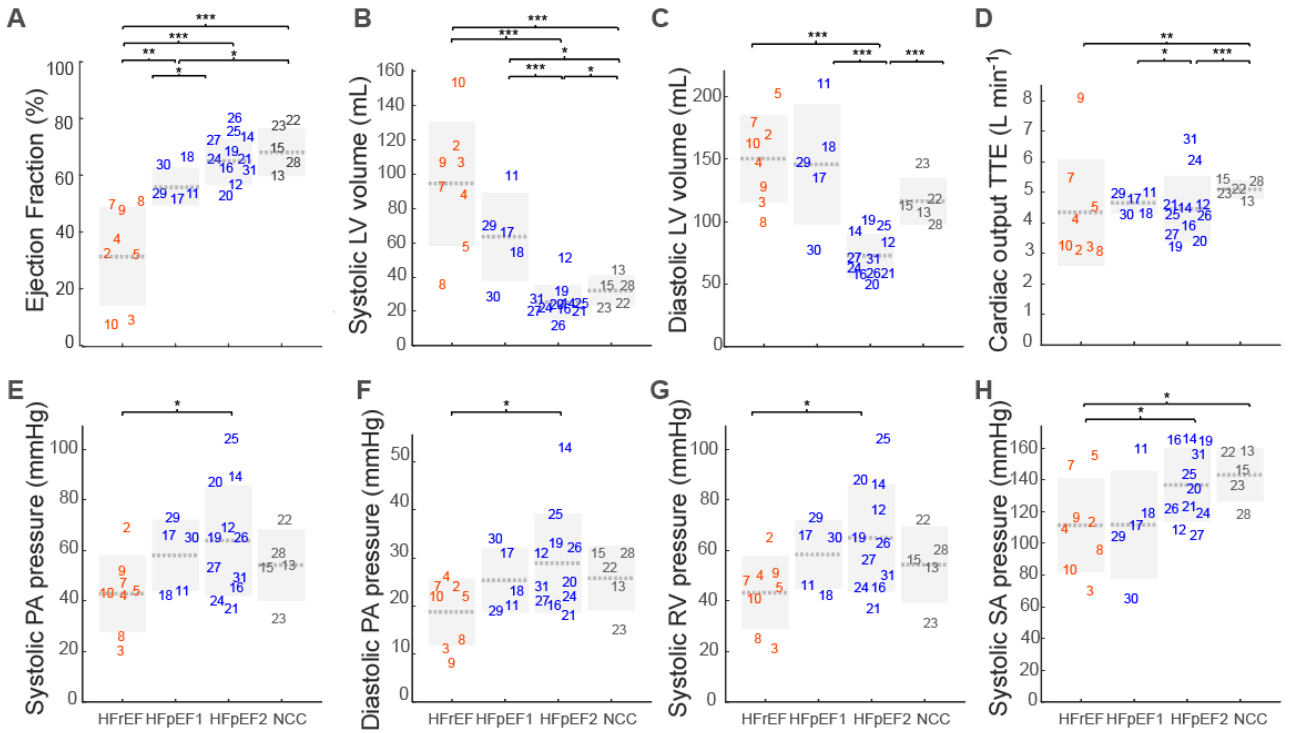
Figure 10. Box plots of the clinical data with 4 heart failure groups with significant differences between heart failure patients based on their HFrEF and HFpEF diagnosis. **A.** Ejection fraction (%). **B.** Systolic left ventricular (LV) volume (mL). **C.** Diastolic LV volume (mL). **D.** Cardiac output (L min^{-1}) from the TTE data. **E.** Systolic pulmonary arterial (PA) pressure (mmHg). **F.** Diastolic PA pressure (mmHg). **G.** Systolic right ventricular (RV) pressure (mmHg). **H.** Systolic systemic arterial (SA) pressure (mmHg). The light gray dashed line denotes the group average, and the grey box contains one standard deviation above and below the mean of each clinical value (*p-value <0.05, **p-value <.01, ***p-value <.001).